

<sup>1</sup>Department of Astronomy, University of Wisconsin, Madison, USA, 53706;  
email: sstanimi@email.edu

<sup>2</sup>Department of Physics, University of Wisconsin, Madison, USA, 53706

# Atomic and Ionized Microstructures in the Diffuse Interstellar Medium

Snežana Stanimirović,<sup>1</sup> Ellen G. Zweibel,<sup>1,2</sup>

Xxxx. Xxx. Xxx. Yyyy. Aa:1–41

[https://doi.org/10.1146/\(\(please add article doi\)\)](https://doi.org/10.1146/((please add article doi)))

Copyright © Yyyy by Annual Reviews.  
All rights reserved

## Keywords

interstellar medium structure, tiny scale atomic structure, tiny scale ionized structure, extreme scattering events, interstellar turbulence

## Abstract

It has been known for half a century that the interstellar medium (ISM) of our Galaxy is structured on scales as small as a few hundred km, more than 10 orders of magnitude smaller than typical ISM structures and energy input scales. In this review we focus on neutral and ionized structures on spatial scales of a few to  $\sim 10^4$  Astronomical Units (AU) which appear to be highly overpressured, as these have the most important role in the dynamics and energy balance of interstellar gas: the Tiny Scale Atomic Structure (TSAS) and Extreme Scattering Events (ESEs) as the most over-pressured example of the Tiny Scale Ionized Structures (TSIS). We review observational results and highlight key physical processes at AU scales. We present evidence for and against microstructures as part of a universal turbulent cascade and as discrete structures, and review their association with supernova remnants, the Local Bubble, and bright stars. We suggest a number of observational and theoretical programs that could clarify the nature of AU structures. TSAS and TSIS probe spatial scales in the range of what is expected for turbulent dissipation scales, therefore are of key importance for constraining exotic and not-well understood physical processes which have implications for many areas of astrophysics. The emerging picture is one in which a magnetized, turbulent cascade, driven hard by a local energy source and acting jointly with phenomena such as thermal instability, is the source of these microstructures.

## Contents

1. INTRODUCTION .....	3
1.1. Fundamentals: The Phases of the Interstellar Medium .....	4
1.2. Interstellar Thermal Pressure Fluctuations .....	5
1.3. Turbulent Fluctuations in the Interstellar Medium .....	7
2. Microstructures in the Neutral ISM .....	8
2.1. Spatial and temporal variability of HI absorption line profiles against non-pulsar sources .....	8
2.2. Temporal variability of HI absorption profiles against pulsars .....	13
2.3. Spatial and temporal variability of optical and ultraviolet lines .....	15
2.4. Theory of Neutral Structures .....	18
2.5. Summary and Outstanding Questions .....	21
3. Tiny Scale Ionized Structure .....	25
3.1. Extreme Scattering Events .....	26
3.2. Theory of Ionized Structures .....	31
3.3. Summary and Outstanding Questions .....	34
4. Future advances, observational and theoretical .....	36

*“If there is the slightest foundation for these remarks the zoology of Archipelagoes will be well worth examining; for such facts (would) undermine the stability of Species.” Charles Darwin, 1836*

## 1. INTRODUCTION

The diffuse interstellar medium (ISM) in the Galaxy contains structure over a wide range of spatial scales. For the neutral medium, a diverse hierarchy of structures on spatial scales  $> 1$  pc has been observed for decades, while the ionized medium has been known to exhibit structure on much smaller spatial scales reaching down to a hundred of kilometers (Rickett 1977; Armstrong, Rickett & Spangler 1995; Haverkorn & Spangler 2013).

The cornerstone of most ISM models is a rough pressure equilibrium between different thermal phases (Ferrière 1998). The coexistence of the multiple phases, however, requires a well-defined, narrow range of thermal pressures  $P/k \sim 3000$  K cm<sup>-3</sup> (see Section 1.2)<sup>1</sup>. Since the late 70s, however, sporadic observations of small-scale ISM structures with highly unusual properties have started to emerge. The Tiny Scale Atomic Structure (TSAS term first introduced by Heiles 1997) has been observed on spatial scales of a few to 10<sup>4</sup> Astronomical Units (AUs) using several different observational techniques at radio and optical/ultraviolet wavelengths, with observationally inferred hydrogen density of  $n_H \sim 10^4$  cm<sup>-3</sup>. At temperatures of 60-260 K, TSAS appears hugely over-pressured with  $P/k \sim 10^6$  K cm<sup>-3</sup>. In the mid 80s the Tiny Scale Ionized Structure (TSIS) was discovered in radio observations of an extreme scattering event (ESE). With even smaller spatial scales, an electron density  $n_e > 100$  cm<sup>-3</sup> at  $T > 1000$  K again implied similarly large thermal pressures. A schematic summary of basic properties of TSIS and TSAS is shown in Figure 1. Their implied thermal pressure is on average at least 100 times higher than the theoretically expected range for the multiphase medium ( $P_{min}$  to  $P_{max}$ ).

These observational results were so mind-boggling that Lyman Spitzer wrote in a letter to Phil Diamond on January 15, 1997: “In view of the revolutionary importance which such structures have in our understanding of the interstellar gas, I am trying to understand the relevant observations and how they are interpreted.” While the abundance of such over-pressured structures is still not well constrained, their story may be somewhat reminiscent of Charles Darwin’s discovery of slightly different forms of mockingbirds and tortoises on the different islands of the Galapagos archipelago, or, to be mundane, the stray thread that when tugged unravels an entire garment.

From the beginning, the study of TSAS and TSIS has been haunted by three interrelated issues: energetics, geometry, and pervasiveness. Attempts to explain the electron density fluctuations which cause pulsar scintillation, the first form of small scale structure discovered (Scheuer 1968), as compressive plasma waves ran into the difficulty that the waves are strongly damped and require a large power source (Scheuer 1968). Although it was not commented upon at the time, the heating resulting from so much dissipation would also be large (§ 3.2.1).

With the discovery of TSAS (Dieter et al. 1976) and extreme scattering events (Fiedler et al. 1987), both hinting at significant overpressures and short relaxation times, the power source problem was exacerbated. At the same time, it was realized that both the energetics and pressure problems can be alleviated if the density structures are highly

<sup>1</sup>We use Gaussian cgs units throughout this paper.

elongated and viewed end on (Romani, Blandford & Cordes 1987; Heiles 1997). Identifying the physical processes that create such structures and quantifying their effects and observational signatures has been a challenging problem. Progress toward solving these problems depends on knowing more about the overall environment in which small scale structure exists. Is it in one of the pervasive phases of the ISM, such as cold neutral or warm ionized gas? Is it an interface phenomenon that occurs in supernova remnant shells, bubble walls, cloud edges, or shocks? Or is there a population of tiny, self gravitating clouds, entities unto themselves? Over time, explanations have coalesced around two poles, one favoring special, discrete structures and the other based on statistical properties of interstellar turbulence.

Understanding of TSAS and TSIS is important as the existence and properties of these structures could be undermining our understanding of heating, cooling and dynamical processes in the ISM, and potentially could lead to the discovery of physical processes that we have yet to account for. In addition, as pointed out by Smith et al. (2013), the existence of small and highly dense regions in the ISM has important implications for interstellar chemistry. At high densities the interstellar radiation field is attenuated, resulting in an enhanced abundance of molecular species. And if, as we discuss later, TSAS and TSIS are associated with strong dissipation, the resulting free energy could power unusual chemistry.

Besides addressing important aspects of the mainstream ISM, AU-scale structure could represent an important bridge to planetary science, and several recent studies have started to explore this avenue. Ray & Loeb (2017) suggested that hydroxyl radical (OH), neutral hydrogen (HI), and other spectral lines offer an exciting way to probe structure on  $\sim 1000$  AU scales around pulsars and search for the planet-building material. Boyajian’s star, an extraordinary star found by Planet Hunters whose properties appear to require TSAS to explain its flux variability, demonstrates the importance of TSAS for future planet searches (Wright & Sigurdsson 2016; Simon et al. 2017).

While we focus in this review on the atomic and ionized microstructure within the Milky Way, observational evidence is starting to emerge about the AU-scale structure in external galaxies. For example, Hacker et al. (2013) studied absorption lines in quasar spectra using the Sloan Digital Sky Survey and found evidence for absorption line variability in the intervening systems on scales 10-100 AU, suggesting that TSAS is likely to exist in host foreground galaxies. Boissé et al. (2015) found structure on similar scales in Mg II and Fe II temporal variability using Very Large Telescope and Keck observations. Finally, there are some indications that even damped Lyman  $\alpha$  absorbing systems at high redshift may contain HI structure on scales of  $\sim 10 - 100$  AU (Kanekar & Chengalur 2001).

In this review, we focus on TSAS and TSIS (mainly traced by extreme scattering events) as these microstructures have a clear over-pressure problem. AU-scale structure has also been observed in the diffuse molecular medium. Considering the intrinsically large pressure of molecular clouds due to self-gravity, magnetic, and surface forces, the over-pressure problem becomes less pronounced for AU-scale molecular structure.

Although literature up through 2017 is cited, the bibliography is not comprehensive, and due to space limitations we had to omit discussion of many important papers. The reader is referred to excellent articles in the ASP Conf. Series Vol. 365 Haverkorn & Goss (2007) for complementary details on optical absorption line studies, or the Galactic tiny-scale structure in the ionized and molecular gas, to preceding ARAA articles on TSIS (Rickett 1990, 1977), and to the recent review by Haverkorn & Spangler (2013).

## 1.1. Fundamentals: The Phases of the Interstellar Medium

The diffuse ISM does not uniformly populate the density-temperature parameter space but is known to exist in several aggregations or phases. Two flavors of the neutral medium exist, corresponding to two phases: the cold neutral medium (CNM) and the warm neutral medium (WNM). Traditionally, the CNM and WNM are understood as being two thermal equilibrium states of the neutral medium (Field, Goldsmith & Habing 1969; McKee & Ostriker 1977; Wolfire et al. 2003). The theoretically expected properties of the CNM and WNM, based on the heating and cooling balance, are: a kinetic temperature  $T_k \sim 60 - 260$  K and a volume density of  $n_H \sim 7 - 70$  cm $^{-3}$  for the CNM<sup>2</sup>, and  $T_k = 5000 - 8300$  K and  $n_H \sim 0.2 - 0.9$  cm $^{-3}$  for the WNM (Wolfire et al. 2003, Table 3 for the Solar neighborhood). The diffuse warm ionized medium (WIM) has  $n_H \sim 0.3$  cm $^{-3}$  and  $T_k \sim 8000$  K, while the hot ionized medium (HIM) has  $n_H \sim 3 \times 10^{-3}$  cm $^{-3}$  and  $T_k \sim 10^6$  K, Draine (2011). The diffuse ISM phases have a roughly comparable thermal pressure (Ferrière 1998). Molecular clouds and HII regions, on the other hand, are often not considered as ISM phases due to their overpressure relative to the four phases. While molecular clouds are

---

<sup>2</sup>We note that CNM temperature can be even lower in the case when dust heating via photoelectric effect is not effective, Spitzer (1978). For example, if cosmic rays and X-rays are the only heating sources, the CNM is expected to have temperature of  $\sim 20$  K (Mark Wolfire, private communication).

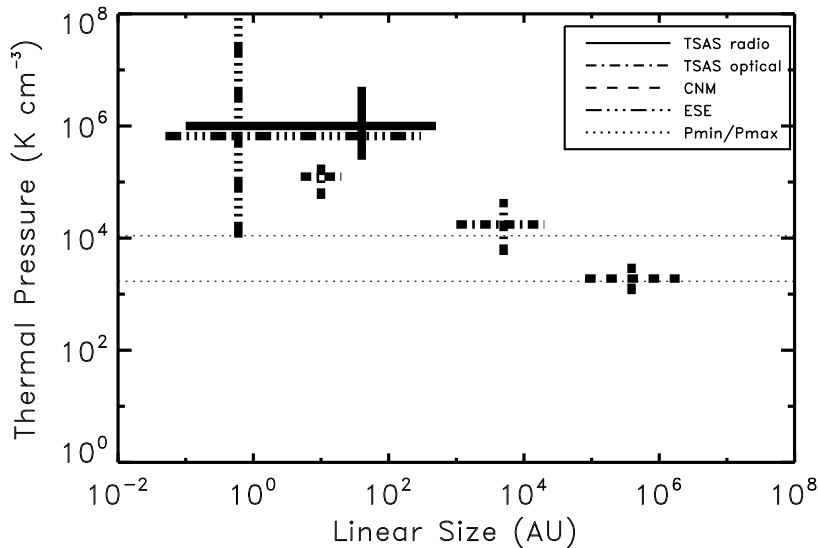


**Figure 1**

A schematic summary of basic properties of TSAS and TSIS we consider in this review. The dotted lines show the rough range of allowed thermal pressures based on Wolfire et al. (2003) and Cox (2005). Properties of the Cold Neutral Medium (CNM) clouds are based on McKee & Ostriker (1977) and Spitzer (1978).

gravitationally confined, HII regions are undergoing expansion.

While the ISM phases are traditionally understood as thermal equilibrium states, more recent ISM models and observations have emphasized the highly dynamic and turbulent character of the ISM and the consequences this has on the fraction of gas outside of the equilibrium states. For example, Audit & Hennebelle (2005) showed that a collision of turbulent flows can initiate fast condensation of WNM into cold neutral clouds with the fraction of cold gas, as well as the fraction of thermally unstable gas, being controlled by turbulence. Koyama & Inutsuka (2002) and Mac Low et al. (2005) explored the importance of shocks driven into warm, magnetized, and turbulent gas by supernova explosions. They found a continuum of gas temperatures, with a fraction of the thermally-unstable WNM being constrained by the star formation rate. The fractions of cold and thermally unstable gas, however, vary widely with numerical models and can depend on input physics but also numerical resolution (Kim, Kim & Ostriker 2008). The question of whether the ISM phases are, on average, in thermal and dynamical equilibrium is still open from both theoretical and observational perspectives (e.g. Heiles & Troland 2003; Begum et al. 2010; Murray et al. 2017) to cite just a few examples.

Two points should be borne in mind when applying the theory of thermal phases to small scale structure. First, coexisting phases are separated by thin fronts in which thermal conduction is important, the temperature is unstable, and gas either evaporates or condenses, depending on pressure. We show in § 2.4 that TSAS is comparable in size to the thickness of these fronts. Second, although pressure fluctuations in a turbulent medium can mediate transitions between phases, the turnover time of a turbulent eddy decreases with spatial scale such that there is a minimum scale at which there is time for heating and cooling processes to operate. Below this scale, the gas is approximately adiabatic.

## 1.2. Interstellar Thermal Pressure Fluctuations

One of the main problems regarding TSAS is its (model-dependent) over-pressure relative to the traditional thermal pressure of the ISM, which suggests that TSAS cannot persist nor be pervasive. We summarize here briefly theoretical and observational pressure constraints.

The theoretical constraints regarding thermal pressure come from the observational finding that the CNM and WNM coexist spatially. For this to happen, considering different heating and cooling processes, requires a well-defined and narrow range of thermal pressures  $P_{min}/k = 2 \times 10^3$  to  $P_{max}/k = 5 \times 10^3$  K cm<sup>-3</sup> (Wolfire et al. 2003; this range

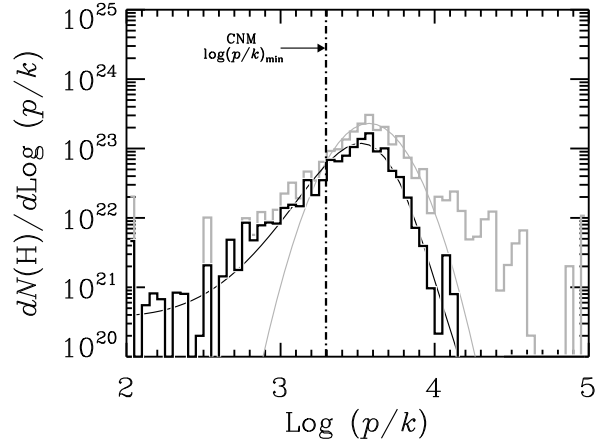


**Figure 2**

The distribution of thermal pressure measurements from Jenkins & Tripp (2011). Two distributions are shown: all measurements in gray, and a sub-sample with  $I/I_0 < 10^{0.5}$  in black. The sub-sample is a better representation of the general ISM away from bright stars. Both distributions were weighted by the hydrogen column density. Lines show fitted expressions provided in Jenkins & Tripp (2011).

corresponds to the Solar neighborhood). Dynamic and turbulent processes can increase the allowed pressure range, however the median thermal pressure of  $P/k \sim 3000 \text{ cm}^{-3}$  is still a good representation (Wolfire 2015).

Several observational studies have measured thermal pressure. Jenkins & Tripp (2011) used ultraviolet spectra of 89 stars to identify three fine-structure lines of atomic carbon C I. They found a median thermal pressure of  $3800 \text{ cm}^{-3}$ , with the central portion of the pressure distribution being fitted with a log-normal function. However, as shown in Figure 2, both low- (at  $P/k < 10^3 \text{ K cm}^{-3}$ ) and high-end ( $P/k > 10^4 \text{ K cm}^{-3}$ ) portions of the pressure distribution showed significant populations. Although the formation and maintenance of the high-pressure regions are open questions, Jenkins & Tripp (2011) argued that such regions are found close to massive stars and are likely affected by dynamical processes like shocks and stellar winds. A small fraction ( $\sim 0.05\%$  by mass) of their measurements have  $P/k > 10^{5.5} \text{ K cm}^{-3}$ . Estimates of *total* pressure, including magnetic fields, cosmic rays, and turbulence are of order  $P/k = 11,000 - 20,000 \text{ K cm}^{-3}$  (Cox 2005), strongly suggesting that the high end of the Jenkins & Tripp distribution cannot be in thermal equilibrium (especially in view of the lower thermal pressures calculated by Wolfire et al. 2003). One possibility, suggested by several studies, is that TSAS traces the high-pressure regions revealed by C I. The under-pressure regions revealed by Jenkins & Tripp observations are also fascinating and potentially important for understanding the TSAS puzzle, we return to this point in § 2.4.

Goldsmith (2013) used ultraviolet CO lines toward nearby stars and found a slightly higher (average) thermal pressure,  $P/k = 4600 - 6800 \text{ K cm}^{-3}$ , while Gerin et al. (2015) used C II observations toward 13 sightlines in the Galactic plane to measure  $P/k = 5900 \text{ K cm}^{-3}$ . Very recently, Herrera-Camus et al. (2017) combined C II and HI observations of nearby galaxies to estimate the C II cooling rate. Their results agree with Jenkins & Tripp (2011), and also confirm the finding that thermal pressure increases with the interstellar radiation field and the star formation activity.

As shown in the schematic figure (Figure 1), according to most interpretations (with the exception of TSIS that causes pulsar scintillation) the column densities and transverse dimensions of both ESEs and TSAS imply very large internal pressure unless the line of sight dimension is much longer than the transverse dimension. This requires either that the structures be self confined or that they are transitory but replenished, in a statistical sense, by a powerful source.

The energy output by freely expanding small scale structures could be considerable. Suppose the structure consists of clouds that survive for time  $\tau_s$ , which for overpressured clouds of size  $l$  and internal velocity dispersion  $v$  would be the free expansion time  $l/v$ . If there are  $n_c$  clouds per unit volume then the pathlength  $\lambda$  that has to be observed for one detection is  $\lambda \sim (\pi n_c l^2)^{-1}$ . That is, if we observe  $N_s$  sources at an average distance  $D_s$  and detect  $X$  small scale structure components, then  $\lambda = N_s D_s / X$ , and the volume filling factor  $f \sim (4/3)l/\lambda$ .

The expansion of a cloud of pressure  $P_c$  injects energy at the rate  $\dot{E} \sim 4\pi P_c l^2 v \sim 4\pi P_c l^3 / \tau_s$ , (assuming that there are no radiative losses). The energy input rate per volume is  $n_c \dot{E} \sim 3P_c f v / l$ . For an overpressure of 100,  $P_c \sim 10^{-11}$

dyn cm<sup>-2</sup> (or  $P_c/k \sim 7 \times 10^4$  K cm<sup>-3</sup>). If  $v \sim 1$  km s<sup>-1</sup> and  $\lambda \sim 10$  AU, the energy input rate is about  $2 \times 10^{-20} f$  erg cm<sup>-3</sup> s<sup>-1</sup>. In comparison, Wolfire et al. (2003) fit the radiative cooling rate of the neutral ISM (their eqn. 3) by the formula  $\Lambda(T) = 1.4 \times 10^{-27} T_2^{0.8}$  erg cm<sup>3</sup> s<sup>-1</sup>, where  $T_2 \equiv T/10^2$  K; this formula is accurate to 35% for  $0.55 < T_2 < 85$  (and  $n$  refers to the mean ambient density, not the TSAS density). The condition that heating by TSAS expansion not exceed radiative cooling is then  $f < 7 \times 10^{-8} T_2^{0.8} n^2$ . For example, if  $T_2 = 0.2 - 1$  and  $n = 100$  cm<sup>-3</sup>,  $f$  must be less than  $(2 - 7) \times 10^{-4}$ . While these numbers are rough and not rigorous, it seems that on energetic grounds the ISM cannot tolerate too large a population of highly overpressured clouds.

### 1.3. Turbulent Fluctuations in the Interstellar Medium

Interstellar turbulence plays a very important role in the ISM, e.g. (Miville-Deschênes et al. 2010; Armstrong, Rickett & Spangler 1995). Turbulence is far too broad a topic to be reviewed here; please see Elmegreen & Scalo (2004); Scalo & Elmegreen (2004); Lazarian et al. (2009) for fairly recent discussions of astrophysical turbulence and a textbook such as Tennekes & Lumley (1972) for basic concepts. Here we only introduce a few central ideas and terms that we will refer to later in the paper. Additional features of turbulence are discussed in §2.4.2.

A *turbulent cascade* refers to motions over a range of spatial scales that are generated nonlinearly by energy input  $\dot{E}$  at a particular scale (for example, a sound wave of wavenumber  $k$  beats with itself to create a sound wave of wavenumber  $2k$ ). If the energy transfer between scales conserves energy, that part of the cascade is called the *inertial range*. Over the inertial range, isotropic turbulence in incompressible gas follows the famous Kolmogorov scaling law according to which  $E_k dk$ , the kinetic energy between wavenumber  $k$  and  $k + dk$ , is proportional to  $k^{-5/3}$  (if we write the integral over wavenumber space in 3 dimensions then  $E_k = 4\pi k^2 P_k$ , where the power spectrum  $P_k \propto k^{-11/3}$ ). If a strong magnetic field is present, motions parallel to it are suppressed relative to perpendicular motions but the perpendicular motions still follow Kolmogorov scaling. The contours of constant power in  $\mathbf{k}$  space are elongated, with  $k_{\parallel}/k_{\perp} \sim (k_d/k_{\perp})^{1/3}$ , where  $k_d$  is the wavenumber at which the turbulence is driven (Goldreich & Sridhar 1995). These properties can be derived by assuming energy conservation together with the concept of “critical balance”, i.e. that the eddy turnover rate  $k_{\perp} v_{k,perp}$  is the same as the frequency of a parallel-propagating Alfvén wave,  $k_{\parallel} v_A$ . In the limit of extreme compressibility we have Burgers turbulence, which is comprised entirely of shocks and has a  $k^{-2}$  energy spectrum. When compressibility is accounted for, subsonic to transonic turbulence is accompanied by density fluctuations with the same power spectrum as the velocity fluctuations, but Kritsuk et al. (2007) found a log normal density fluctuation spectrum in numerical simulations of isothermal hydrodynamic turbulence with Mach number 6.

If energy is dissipated by a process such as viscosity which increases with decreasing scale, then the inertial range terminates at the scale where the dissipation rate equals the energy transfer rate. For Kolmogorov turbulence this scale is  $l_K \sim (\rho \nu^3 / \dot{E})^{1/4}$ , where  $\nu$  is the kinematic viscosity. The cascade at scales below the inertial range is called the *dissipation range*, and typically cuts off exponentially.

Many studies have observed the turbulent spatial power spectrum down to spatial scales of  $\lesssim 1$  pc using many different tracers (Elmegreen & Scalo 2004). The slope of the 3D power spectrum depends on the interstellar tracer, optical depth, and velocity resolution. For example, the electron density fluctuations follow a Kolmogorov spectrum over the range of scales from  $\sim 30$  pc to  $\sim 70$  km (Armstrong et al. 1995, see Section 3). A 3D power spectrum slope of  $-3.7$  was measured for the warm, optically-thin, Galactic HI seen in emission (Dickey et al. 2000), or  $\sim -3$  for HI in an optically-thick region close to the Galactic plane in agreement with theoretical expectations for the optically-thick medium (Lazarian & Pogosyan 2004). Several carbon monoxide (CO) studies of even denser and optically-thick medium have found an even flatter slope of  $-2.8$  (Stutzki et al. 1998). Miville-Deschênes et al. (2010) derived a spatial power spectrum of dust column density fluctuations in the Polaris flare region over the range of scales from  $\sim 2000$  AU to  $\sim 20$  pc and found a slope of  $-2.7$ . It is expected that interstellar turbulence extends further down even to smaller spatial scales (Hennebelle & Falgarone 2012). However, the nature of dissipation processes, spatial scales on which they operate, and the local heating induced by turbulent dissipation, are complex questions that still need to be constrained observationally.

Several studies have hypothesized that TSAS could be related to the turbulent energy cascade on larger scales and possibly even trace the tail-end of the turbulent spectrum. For example, Deshpande (2000) suggested that the optical depth variations ascribed to TSAS are primarily due to contributions from the large scale end of the interstellar turbulent cascade, thereby circumventing the overpressure problem. We discuss this further in § 2.4.

As mentioned above, turbulence in a strong magnetic field is anisotropic, with elongated eddies. In estimating number densities from column density of TSAS and TSIS it is often assumed that the line of sight and transverse dimensions are similar. As pointed out by Heiles (1997), the inferred densities and pressures would be lower if

TSAS/TSIS were filaments viewed edge on. The connection to magnetized turbulence is not straightforward, however, because the cascade described above is incompressible. The incompressible cascade does generate density fluctuations of an amplitude that scales with Mach number, but they are isotropic (Cho & Lazarian 2003) and do not produce elongated structures. There is direct evidence for anisotropic TSIS structures (Armstrong, Cordes & Rickett 1981). A recent study by Kalberla & Kerp (2016) found evidence for anisotropy in the HI spatial power spectrum for an intermediate latitude Galactic field. While the spectral index of the power spectrum remained close to Kolmogorov value, the spectral power changed with the position angle.

## 2. Microstructures in the Neutral ISM

The Tiny-Scale Atomic Structure or TSAS has been observed in the ISM for over four decades using many different observational approaches. In the radio, spatial and temporal variability of HI absorption line profiles in the direction of background non-pulsar sources (summarized in Section 2.1) have been used extensively. Extragalactic compact and resolved, single or multiple, radio continuum sources are commonly used as non-pulsar targets. Several Galactic supernova remnants have been used as extended background sources to map out the distribution of the absorbing HI. One Galactic microquasar was also used as a target for temporal observations. Pulsars have several unique characteristics that make them especially exciting as targets for the temporal variability of absorption profiles, as discussed in Section 2.2. Finally, several different approaches have been used to study spatial and temporal variability of optical and ultraviolet absorption lines and we summarize main results in Section 2.3. We summarize key observational results from the HI absorption studies in Table 1 (non-pulsar sources) and Table 2 (pulsar sources) and list basic observed quantities of TSAS provided in the literature. We also provide in these tables the assumptions, such as distance to the absorbing medium and temperature, when available, with a goal of providing a complete data set for future uses. For completeness, we list both detections and non-detections. Several theoretical models and important questions about TSAS are outlined in Section 2.4.

### 2.1. Spatial and temporal variability of HI absorption line profiles against non-pulsar sources

**2.1.1. Early Studies.** As irregularities in the ionized interstellar gas have been known to exist down to very small spatial scales,  $\sim 10^7$  cm, Dieter, Welch & Romney (1976) were the first to ask the question whether irregularities in the neutral medium could extend to similarly small scales. Single, long baseline interferometric (VLBI) observations of the quasar 3C147 showed variations in the HI absorption line profiles with interferometric hour angle. Dieter et al. (1976) interpreted these variations as being due to inhomogeneities of the absorbing medium. If resulting from a discrete cloud, the measured difference in optical depth profiles  $\Delta\tau$  implied a cloud HI column density of  $N(HI) = 10^{20}$  cm $^{-2}$  using:

$$N(HI) = C_0 \times T_s \times \int \Delta\tau dv \quad (1)$$

where  $C_0 = 1.823 \times 10^{18}$  cm $^{-2}$  K $^{-1}$  (km/s) $^{-1}$  and  $T_s$  is the excitation or spin temperature (the exact values for temperature and distance used in calculations are given in Table 1). The velocity in this equation corresponds to radial velocity along the line of sight. The maximum separation of source components of 0.16", implied a cloud size of  $l = 70$  AU and a HI volume density of  $n_H = N(HI)/l = 10^5$  cm $^{-3}$  (assuming spherical geometry). The over-dense and over-pressured TSAS was born! Subsequent VLBI observations by Diamond et al. (1989) found change in HI absorption spectra when varying angular resolution, implying evidence for 25-AU HI clouds in directions toward 3C138, 3C380, and 3C147. Particularly large variations were noticed in the case of 3C138, suggestive of TSAS with  $n_H = (5 - 10) \times 10^4$  cm $^{-3}$ . This study raised the questions regarding the filling factor, confinement, and regeneration mechanisms for such over-dense and over-pressured structures, and suggested that a continuous range of optically thick cloudlets with sizes of tens of AUs may exist in the ISM.

The first *images* of the HI optical depth distribution in the direction of extragalactic sources were obtained by Davis, Diamond & Goss (1996) toward 3C138 and 3C147, using the MERLIN array and the European VLBI Network, detecting significant optical depth fluctuations (Table 1). Faison et al. (1998) imaged 3C 138, 2255+416, and 0404+768 at even higher angular resolution of 10-20 mas using the Very Long Baseline Array (VLBA). They found optical depth variations for the first two sources. As 0404+768 did not show fluctuations over spatial scales probed (3–16 AU), they suggested a possible minimum size for TSAS structures of a few tens of AU. Faison & Goss (2001) used the VLBA to extend their previous study to seven sources in total. They observed 3C147, 3C119, CJ1 2352+495 and CJ1 0831+557 with an angular resolution of 5 mas, confirming only optical depth variation in the case of 3C147 (Table 1). They also used Zeeman splitting to estimate the upper limit on the (absolute) strength of the



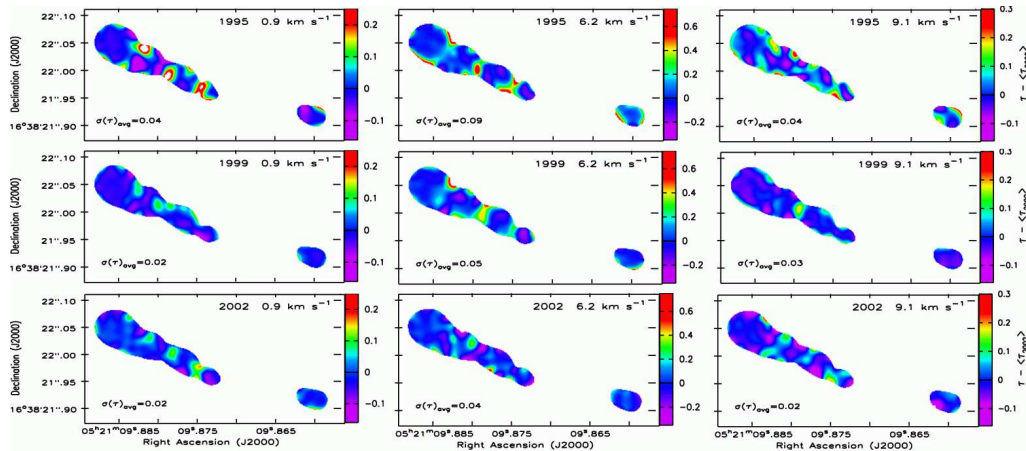


Figure 3

The HI optical depth variability in the direction of 3C138 from Brogan et al. (2005). Images show the optical depth at three different velocities for three epochs. The the average value of the 2002 optical depth was subtracted from each image. The color scale has been adjusted so that the dark blue color is centered about zero. The average  $1\text{-}\sigma$  uncertainty is indicated in the bottom left corner of each panel.

line-of-sight magnetic field of  $32 \mu\text{G}$  for 3C147,  $20 \mu\text{G}$  for 3C119, and  $160 \mu\text{G}$  for 2352+495, suggesting that the field is not enhanced towards these sources. However, considering a typical line-of-sight field of  $\sim 6 \mu\text{G}$  (Heiles & Troland 2005), the obtained upper limits are clearly very high and further magnetic field measurements are highly needed.

In summary, while spatial variability of HI absorption profiles against extragalactic sources found clear TSAS examples, since early days TSAS was not seen in all observed directions. Faison et al. (1998) was the first to question whether the absence of TSAS on spatial scales below few tens of AU has a physical meaning. While most sources showed  $\Delta\tau < 0.1$ , 3C138 and 3C147 showed much higher level of variability.

**2.1.2. The Highly Variable 3C138 and 3C147 Directions.** While several early observations showed significant optical depth variability in the direction of 3C138 and 3C147, Brogan et al. (2005) and Lazio et al. (2009) remain as studies with the most exquisite HI optical depth images against these sources. Brogan et al. (2005) imaged 3C138 in a three-epoch series of observations (1995, 1999 and 2002), and showed clear evidence for spatial variations of typically  $\Delta\tau \sim 0.1$  (and reaching a maximum value of 0.5) on scales of 25 AU, Figure 3. In addition, *temporal* changes in the HI optical depth images have been found over a period of 7 years, with implied transverse velocity for the intervening HI of order  $20 \text{ km s}^{-1}$ . In a followup study, Lazio et al. (2009) obtained VLBA HI absorption images of 3C147 and found optical depth variations on typical scales of 10 AU (or 15 mas) with  $\Delta\tau \sim 0.1 - 0.3$  (reaching a maximum value of 0.7).

One possible way of mitigating the over-pressure problem of TSAS is if its spin temperature,  $T_s$ , is significantly lower relative to the typical CNM clouds ( $\sim 15 \text{ K}$ , Heiles 1997). Brogan et al. (2005) compared line widths of HI absorption spectra between VLBA and Heiles & Troland (2003) Arecibo observations of 3C138 and found excellent agreement. By assuming that linewidths are thermal in nature, they suggested that TSAS does not have significantly lower temperature than the typical CNM. However, we note that turbulent broadening can dominate over thermal broadening, resulting in the above experiment being inconclusive. Therefore, the question of how TSAS compares to the CNM regarding its temperature still remains as open. For one of the velocity components in the direction of 3C138,  $6.4 \text{ km/sec}$ , Heiles & Troland (2004) estimated  $B_{los} = +5.6 \pm 1.0 \mu\text{G}$ . This is in agreement with the median total magnetic field (e.g. Heiles & Troland 2005) supporting earlier suggestions that TSAS likely does not reside in regions with an enhanced magnetic field strength and consistent with the theoretical arguments in § 2.4.

Brogan et al. and Lazio et al. estimated the volume filling factor of TSAS in the direction of both 3C147 and 3C138 as being  $\lesssim 1\%$ . This is in agreement with a few percent volume filling factor of the over-pressured ISM estimated by Jenkins & Tripp (2001), and such structures are expected to be far from equilibrium and short-lived. However, according to the energy input argument given in §1.2, the energy input from free expansion of such structures would be of order  $2.0 \times 10^{-22} (P_c/10^{-11})(v_5)(10 \text{ AU}/l) \text{ erg cm}^{-3}\text{s}^{-1}$ , where the units of pressure and velocity are in dyne  $\text{cm}^{-2}$  and  $\text{km s}^{-1}$ . Although this is an upper limit, the volume filling factor of 1% implies that this heating rate can only be balanced by radiative cooling for  $n > 370/T_2^{0.4} \text{ cm}^{-3}$ , which is very high for the CNM. This large heating rate would affect many areas of astrophysics, and would have a detectable effect on temperature of dust grains and

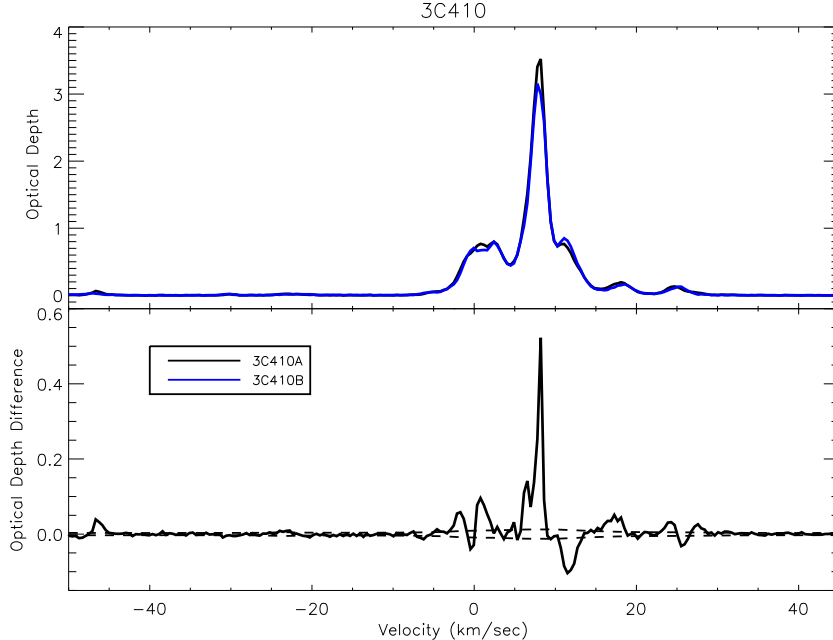


**Figure 4**

(Top) HI absorption spectra in the direction of radio continuum sources 3C410A and 3C410B from the 21-SPONGE survey shown in black and blue. The two components (A and B) in this double source are separated by only  $5.4''$ . At the assumed distance of  $0.1/\sin b = 1.5$  kpc, the separation between two components corresponds to a linear distance of  $\sim 8,000$  AU. (Bottom) The difference of two HI optical depth profiles. Dashed lines show the  $1\text{-}\sigma$  uncertainty. The maximum  $\Delta\tau = 0.5$  is found at a radial velocity of  $\sim 8$  km/s.

HI clouds.

While both studies claimed that sightlines to 3C138 and 3C147 are not special, previous HI emission observations of 3C147 by Kalberla, Schwarz & Goss (1985) found HI at 500-2000 K – this thermally unstable HI likely signals possible dynamical events in the recent history of the region. In addition, we note that both directions have significant HI column density:  $\sim 6 \times 10^{21} \text{ cm}^{-2}$  for 3C138 and  $\sim 8 \times 10^{20} \text{ cm}^{-2}$  for 3C147. This is higher than the column density of typical diffuse lines of sight and is similar to what is typically found close to molecular clouds (Stanimirović et al. 2014). Such column densities may have enough shielding for  $\text{H}_2$  formation, e.g. Lee et al. (2012), and could signal the presence of a denser, more clumpy medium.

Brogan et al. suggested that TSAS is ubiquitous in the ISM. Their explanation for the lower observed levels of variations in the cases of sources other than 3C138 and 3C147 is based on selection effects, e.g. other sources have a smaller angular extent and lower surface brightness, resulting in a smaller dynamic range of probed spatial scales. However, the typical size of TSAS structures found for both 3C138 and 3C147 is only 2-2.5 times larger than the telescope beam (although observations were sensitive to a continuous range of spatial scales from 20 to 300 mas). Future observations with a broader observed range of TSAS sizes are needed to confirm this interpretation.

In summary, 3C138 and 3C147 have shown significant spatial and temporal variations of HI optical depth over several studies. TSAS features in these two directions show interesting similarities. TSAS volume filling factor is  $\sim 1\%$ , however no clear observational constraints of the TSAS temperature exist to date. We caution that in both cases, the typical TSAS size found is very close to the linear resolution of VLBA observations. Both directions have the total HI column density similar to what is found close to molecular clouds, suggesting suitable conditions for the formation of  $\text{H}_2$ . As many numerical simulations suggest  $\text{H}_2$  formation via converging flows (e.g. Hennebelle, Audit & Miville-Deschênes 2007), both lines of sight could be undergoing a post-shock phase transformation which is characterized by out-of-equilibrium physical properties. If this is the case, then such a level of optical depth variations may not be typical for the ISM. Future observations should search for velocity signatures of converging flows or other dynamical imprints on the velocity spectra.

**2.1.3. Additional Sources.** Dhawan, Mirabel & Rodríguez (2000) used an exotic source - a microquasar GRS

**Table 1 Summary of TSAS radio detections and non-detections for non-pulsar sources.**

Source	Coords (°)	Size (AU)	$\Delta\tau$	$N$ (cm <sup>-2</sup> )	Comment
3c147 <sup>a</sup>	161.69,10.30	70	-	10 <sup>20</sup>	$d = 600$ pc, $T_s = 50$ K
several <sup>a</sup>	-	-			no detection
3c138 <sup>b</sup>	187.5,-11.3	25		10 <sup>19.6</sup>	$d = 500$ pc, $T_s = 50$ K
3c147 <sup>b</sup>	161.69,10.30	25	some		
3c380 <sup>b</sup>	77.23, 23.50	25	some		
3c138 <sup>c</sup>	187.5,-11.3	-	0.16,0.35		
3c147 <sup>c</sup>	161.69,10.30	-	0.07		
3c138 <sup>d</sup>	187.5,-11.3		0.6-0.8		
2255+416 <sup>d</sup>	101.23,-16.11		some		
0404+768 <sup>d</sup>	133.41,18.33	3-16			no detection
3c147 <sup>e</sup>	161.69,10.30		0.28,0.2		$d = 1, 0.5$ kpc
3c119 <sup>e</sup>	160.96,-4.34	10-100	< 0.2		$d = 1.3$ kpc
2352+495 <sup>e</sup>	113.71,-12.03	5-40	< 0.1		
0831+557 <sup>e</sup>	162.23,36.56	30	< 0.1		
3C138 <sup>f</sup>	187.5, -11.3	25	0.1 ± 0.05	10 <sup>19.5</sup>	$d = 500$ pc, $v_{ch} = 0.82$
3C147 <sup>g</sup>	161.69, 10.30	10	0.2 ± 0.07	10 <sup>19.7</sup>	$d = 750$ pc, $v_{ch} = 0.4$
3C161 <sup>h</sup>	215.44,-8.07	450	1.25 ± 0.25	10 <sup>20.5</sup>	$d = 1.8$ kpc, $v_{ch} = 0.49$
3C123 <sup>h</sup>	170.58,-11.66	107	0.7 ± 0.25	10 <sup>20.3</sup>	$d = 530$ pc, $v_{ch} = 0.49$
3C111 <sup>h</sup>	161.68,-8.82	42000	0.3	10 <sup>19.9</sup>	
GRS1915 <sup>i</sup>	45.37,-0.22	900	0.67		55 km/s, $d = 6.1$ kpc, $v_{ch} = 2.6$
GRS1915 <sup>i</sup>	45.37,-0.22	440	0.24		5 km/s, $d = 11$ kpc, $v_{ch} = 2.6$
GRS1915 <sup>i</sup>	45.37,-0.22	150-900	< 0.5		55 km/s, $d = 6.1$ kpc, $v_{ch} = 2.6$
GRS1915 <sup>i</sup>	45.37,-0.22	275-1650	< 0.25		5 km/s, $d = 11$ kpc, $v_{ch} = 2.6$
3C405 <sup>j</sup>	76.2,5.7	206265.	0.13		$d = 1.1$ kpc, $v_{ch} = 2.75$
six other <sup>j</sup>		6000-77000	< 0.03 - 0.2		no detections
3C018 <sup>k</sup>	118.62,-52.73	6077	0.095 ± 0.007		$v_{ch} = 0.4$
3C041 <sup>k</sup>	131.38,-29.07	4772	0.036 ± 0.007		$v_{ch} = 0.4$
3C111 <sup>k</sup>	161.68,-8.82	78649	0.377 ± 0.008		$v_{ch} = 0.4$
3C123 <sup>k</sup>	170.58,-11.66	10631	0.105 ± 0.0035		$v_{ch} = 0.4$
3C225 <sup>k</sup>	220.01,44.01	692	0.040 ± 0.004		$v_{ch} = 0.4$
3C245 <sup>k</sup>	233.12,56.30	530	< 0.02		$v_{ch} = 0.4$
3C327.1 <sup>k</sup>	12.18,37.01	1946	0.093 ± 0.012		$v_{ch} = 0.4$
3C409 <sup>k</sup>	63.40,-6.12	5516	0.275 ± 0.007		$v_{ch} = 0.4$
3C410 <sup>k</sup>	69.21,-3.77	8155	0.523 ± 0.013		$v_{ch} = 0.4$

Column 2 - source Galactic coordinates in degrees. Column 3 - spacial scale of TSAS in AU. Column 4 -variation in HI optical depth. Column 5 - HI column density in cm<sup>-2</sup>. Column 6 - comments include assumed TSAS distance and spin temperature, when provided. The velocity resolution is listed as  $v_{ch}$  as it is important to place all measurements on the same scale. References: <sup>a</sup> - Dieter, Welch & Romney (1976); <sup>b</sup> - Diamond et al. (1989); <sup>c</sup> - Davis, Diamond & Goss (1996); <sup>d</sup> - Faison et al. (1998); <sup>e</sup> - Faison & Goss (2001); <sup>f</sup> - Brogan et al. (2005); <sup>g</sup> - Lazio et al. (2009); <sup>h</sup> - Goss et al. (2008); <sup>i</sup> - Dhawan, Mirabel & Rodríguez (2000); <sup>j</sup> - Dickey, Salpeter & Terzian (1979); <sup>k</sup> - Murray et al. (2015)

1915+105 with a proper motion of 8-17 mas day<sup>-1</sup> - to look for temporal changes in HI absorption spectra. At two different radial velocities, they found significant optical depth variations (for details see Table 1). Goss et al. (2008) used MERLIN to obtain interferometric imaging of three sources: 3C111, 3C123 and 3C161. In the case of 3C161 and 3C111 they found significant optical depth variations on spatial scales of ~ 400 – 500 AU and ~ 42,000 AU, respectively. 3C111 is especially interesting as the same source showed variability in H<sub>2</sub>CO absorption by Moore & Marscher (1995). On the other hand, 3C123 showed only hints of variability at a low statistical significance.

To probe even larger spatial scales of > 10,000 AU (often studied with optical absorption against stars in clusters), observations of double-component extragalactic radio sources can be used. Dickey, Salpeter & Terzian (1979) obtained interferometric HI absorption observations in the direction of 9 double sources and found a significant difference in 3 sources with one source (3C405) being especially convincing with  $\Delta\tau \sim 0.13$  at an upper limit for the linear scale of

**Table 2** Summary of TSAS radio detections and non-detections for pulsars.

Source	Coords ( $^{\circ}$ )	Size (AU)	$\Delta\tau$	$N$ ( $\text{cm}^{-2}$ )	Comment
PSR B1821+05 <sup>a</sup>	34.99,8.86	75	$2 \pm 0.85$		$v_{ch} = 1.2$
PSR B1557-50 <sup>b</sup>	330.7,1.6	1000	1.1		$v_{ch} = 6.7$
PSR B1154-62 <sup>b</sup>	296.71,-0.20				no detection
PSR B1557-50 <sup>c</sup>	330.7,1.6	1000	$0.15 \pm 0.05$		$d = 6.4$ kpc, $v_{ch} = 7.3$
three other PSRs <sup>c</sup>		50-100	$< 0.02 - 0.12$		no detection
six PSRs <sup>d</sup>		5-100	0.03-0.7	$10^{19-20.7}$	$T_s = 50$ K
PSR B0301+19 <sup>e</sup>	49.20,2.10	500	$0.15 \pm 0.01$		$v_{ch} = 2$
two PSRs <sup>e</sup>			$< 0.018 - 0.14$		no detection
PSR B0329+54 <sup>f</sup>	144.99,-1.22	0.005-25	$< 0.026$		no detection
PSR B1929+10 <sup>g</sup>	47.38,-3.88	6.	$0.150 \pm 0.008$	$10^{19.1}$	$T_s = 170$ K, $v_{ch} = 1.04$
PSR B1929+10 <sup>g</sup>	47.38,-3.88	12.	$0.025 \pm 0.008$	$10^{19.4}$	$T_s = 170$ K, $v_{ch} = 1.04$
PSR B1929+10 <sup>g</sup>	47.38,-3.88	28.	$0.020 \pm 0.008$	$10^{19.1}$	$T_s = 170$ K, $v_{ch} = 1.04$
PSR B1929+10 <sup>g</sup>	47.38,-3.88	46.	$0.020 \pm 0.008$	$10^{19.4}$	$T_s = 170$ K, $v_{ch} = 1.04$
PSR B2016+28 <sup>g</sup>	68.10,-3.98	1-10	$< 0.1 - 0.2$		$v_{ch} = 1.04$
PSR B0823+23 <sup>g</sup>	196.96,31.74	5-50	$< 0.01 - 0.02$		$v_{ch} = 1.04$
PSR B1133+16 <sup>g</sup>	241.90,69.19	20-170	$< 0.01 - 0.02$		$v_{ch} = 1.04$
PSR B1737+13 <sup>g</sup>	37.08,21.68	20-180	$< 0.1 - 0.2$		$v_{ch} = 1.04$

Same as in Table 1. References: <sup>a</sup> - Clifton et al. (1988); <sup>b</sup> - Deshpande et al. (1992); <sup>c</sup> - Johnston et al. (2003); <sup>d</sup> - Frail et al. (1994); <sup>e</sup> - Weisberg et al. (2008); <sup>f</sup> - Minter, Balsler & Kartaltepe (2005); <sup>g</sup> - Stanimirović et al. (2010)

HI optical depth fluctuations of  $\sim 1 \text{ pc}^3$ . This study, however, concluded that small-scale HI optical depth structures are uncommon, supporting the validity of 21-cm spin temperature measurements using beam switching.

Very recently, 21-SPONGE has obtained HI absorption spectra in the direction of 52 radio continuum sources with the VLA at exceptional sensitivity,  $\sigma_{\tau} < 0.001$  per 0.4 km/s channels (Murray et al. 2015). Out of 52 sources 8 sources are doubles and one is a triple. This provides a unique opportunity to look for HI optical depth differences at close separations. Of these nine sources eight show significant differences on spatial scales from 700 to 79,000 AU, with  $\Delta\tau$  ranging from 0.04 to 0.5 (Stanimirovic et al., in prep) and a tendency for larger variations to be found at larger spatial separations. As an example, we show the case of 3C410A/B in Figure 4. We note excellent agreement for 3C111 between this study and Goss et al. (2008), while 3C123 observed by Goss et al. had a higher  $\Delta\tau$ .

A new type of HI structures, potentially related to larger TSAS, was discovered recently by Clark, Peek & Putman (2014) by applying the Rolling Hough Transform on the HI emission observations. These linear HI features, named ‘‘HI fibers’’, likely trace the CNM at spatial scales  $< 10^4$  AU,  $N(\text{HI}) \sim 5 \times 10^{18}$ , and are oriented along the magnetic field lines. Clark, Peek & Putman (2014) suggest that HI fibers are likely associated with the Local Bubble wall.

Finally, we note that Dieter-Conklin (2009) emphasized the idea by Marscher, Moore & Bania (1993) that due to the Earth’s motion around the Sun, the Solar motion in the Galaxy, and the cloud’s proper motion, our line of sight to a distant background source is continuously (slowly) moving and we are sampling an intervening ISM at different locations. While this line-of-sight (or ‘‘searchlight’’) wandering still samples TSAS, the main point is that observations are tracing varying sightlines in an interstellar cloud, as opposed to the same sightline where physical properties of the cloud have changed over time. This agrees with the Deshpande (2000) idea that observations at different epochs are sampling a point on the structure function not the power spectrum of optical depth fluctuations.

**2.1.4. Power Spectrum of the HI Optical Depth.** While most reported studies used discrete (or limited) measurements of the HI optical depth and did not have high enough spatial dynamic range to calculate the power spectrum, several direct measurements of the  $\tau$  power spectrum exist to date. Using the SNR Cassiopeia A (or Cas A) as an extended background source, Deshpande, Dwarakanath & Goss (2000) measured the spatial power spectrum of the HI optical depth images ( $\tau(v)$ , as well as  $\int \tau(v) dv$ ) over several different velocity ranges and found a slope of  $2.75 \pm 0.25$  over a range of spatial scales from 0.07 to 3  $\text{pc}^4$ . For Cygnus A they found similar slope for the Outer Arm, while an even more shallow slope of 2.5 for the Local Arm. This power-law index for Cassiopeia A, obtained with the VLA,

<sup>3</sup>This study and many others derived the upper limit on the distance of the absorbing TSAS as:  $110 \text{ pc}/\sin|b|$ , by assuming the CNM scale-height of 110 pc.

<sup>4</sup>A distance of 2 kpc was assumed for the Perseus arm.

was later confirmed in an independent experiment by Roy et al. (2010) using the Giant Metrewave Radio Telescope. Several observational studies have claimed the observed  $\Delta\tau$ , or upper limits, in agreement with the Cas A optical depth spectrum when extrapolated down to  $\sim 100$  AU (Dhawan, Mirabel & Rodríguez 2000; Faison & Goss 2001; Johnston et al. 2003).

Roy et al. (2012) combined VLBA, Merlin and VLA interferometric observations of 3C138 to probe a range of angular scales from 10 mas to  $0.2''^5$ . They calculated a structure function of the HI optical depth images,  $\tau(v)$ , for individual velocity channels and found a corresponding power-spectrum slope of  $2.33 \pm 0.07$ . No significant channel-to-channel variations of the structure-function slope were found. Dutta et al. (2014) used the same data set but with Monte Carlo simulations to assess the effect of low S/N data on the structure function slope. They found a slightly steeper slope,  $2.81_{-0.13}^{+0.14}$ , in excellent agreement with the Deshpande et al. (2000b) Cas A results on much larger scales.

Combining results for these three different regions (Cas A, Cygnus A and 3C138) hint at a possibly similar power spectrum slope of the HI optical depth over a range from 5 AU to 3 pc, which is impressively six orders of magnitude! This result clearly needs to be confirmed and additional observations obtained to bridge the current gap that exists on spatial scales  $\sim 10^2$  to  $\sim 10^4$  AU. Extrapolation of the HI optical depth power spectrum to very small scales has been one of the key criticisms of the Deshpande (2000) model - the measured structure function slope in the direction of 3C138 at least somewhat resolves this concern. However, the question of whether the same slope applies for the cold HI throughout the whole Milky Way still remains. As Brogan et al. (2005) noticed, a small change in the slope of just 0.1 implies a change in the optical depth variations of a factor of 2. Therefore testing the uniformity of the structure function slope with future measurements is very important.

Deshpande, Dwarakanath & Goss (2000) argue that the slopes of the power spectra of relative density fluctuations  $\delta n_H/n_H$  and optical depth variations  $\Delta\tau/\tau$  are the same (this argument assumes both are small). The fraction of mass  $\delta M(< l)/\delta M$  in fluctuations of size  $< l$  for any scale  $l$  within the spectrum is related to the power law index  $q$  by  $\delta M(< l)/\delta M \sim (l/l_{max})^{q+2} = (l/l_{max})^{4.75}$ . That is, the mass in fluctuations is dominated by the largest fluctuations.

## 2.2. Temporal variability of HI absorption profiles against pulsars

There are several reasons why pulsars have been recognized as ideal sources for studying TSAS. First, pulsars have a relatively high proper motion and transverse speeds (typically  $\sim 10 - 100$  AU yr $^{-1}$ ), sampling the CNM on AU spatial scales by obtaining absorption profiles at different epochs. Second, the pulsed nature of pulsars' emission allows spectra to be obtained *on* and *off* source without moving the telescope, therefore sampling both emission and absorption along almost exactly the same line of sight (Stanimirović et al. 2010). With radiative transfer, the on- and off-source spectra can then be used to estimate  $T_s$ . Third, the compact nature of pulsars samples the gas with an effective absorption beam that is limited only by interstellar scattering (see Section 3). This typically gives resolution of 0.1-1 mas (Dickey, Crovisier & Kazes 1981). However, the compact nature of pulsars, as well as their variable nature, require sophisticated fast-sampling spectrometers and careful data processing. For example, interstellar scintillation can cause baseline ripples, while the varying source nature can lead to "ghost effects" (artificial absorption features, Weisberg, Rankin & Boriakoff 1980), which need to be removed.

A unique and exceptionally important aspect of pulsars is that they can be used to probe neutral, ionized, and molecular medium along *identical* lines of sight. This is especially interesting as high-density TSAS may contain molecules, and/or have ionized outer layers that could be observed as dispersion measure (DM) variations. While HI has been studied in absorption using pulsars for several decades, recent studies have detected OH in absorption against several pulsars (Stanimirović et al. 2003; Weisberg et al. 2005). Only two studies have so far obtained simultaneous measurements of HI absorption and dispersion measure (Frail et al. 1994). This is clearly an open area where important progress can be made in the future.

**2.2.1. Early Studies.** In the late 1980s, sufficiently accurate and repeated measurements of HI absorption profiles against pulsars began to be made, and it was noticed that pulsar ISM spectra changed over time in some cases, suggesting inhomogeneities in the intervening gas. For example, Clifton et al. (1988) found that the HI absorption spectrum of PSR B1821+05 changed between  $\sim 1981$  and 1988 by  $\Delta\tau \sim 2$ . Frail et al. (1991) noticed large optical depth variations towards the same pulsar. Deshpande et al. (1992) showed that between  $\sim 1976$  and 1981, HI absorption toward B1154-62 did not change significantly; while toward B1557-50, a variation with  $\Delta\tau \sim 1.1_{-0.6}^{+1.1}$  was interpreted as a TSAS of size in the 1000 AU range.

<sup>5</sup>They used a distance of 500 pc which results in the range spatial scales of 5-100 AU.

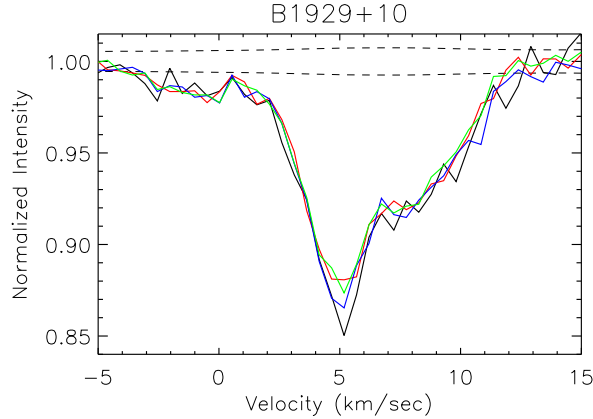


**Figure 5**

HI absorption spectra in the direction of B1929+10 obtained with the Arecibo telescope at four observing epochs. Dashed lines show a typical,  $\pm 1 - \sigma$  noise level in the absorption spectra. The absorption feature at 5 km s<sup>-1</sup> has changed significantly (2-3- $\sigma$  level) with time (Stanimirović 2009; Stanimirović et al. 2010).

The early pulsar HI results inspired Frail et al. (1994) to undertake the first dedicated multi-epoch pulsar HI absorption experiment at Arecibo. Six pulsars were observed at three epochs, probing spatial scales 5–100 AU. These authors reported the presence of *pervasive* variations with  $\Delta\tau \sim 0.03 - 0.7$  for all six pulsars. They indicated that TSAS could comprise 10-15% of the cold ISM. For one of the Frail et al. (1994) pulsars, B0823+26, DM variations of +0.0013 pc cm<sup>-3</sup> were measured by Phillips & Wolszczan (1991) at the same time as HI absorption. DM variations correspond to  $\delta N_{H^+} = 4 \times 10^{15}$  cm<sup>-2</sup>, the level much smaller than the observed variation in HI column density of  $\delta N_{HI} = -5.5 \times 10^{18}$  cm<sup>-2</sup>. Their conclusion was that DM variations are smooth in this direction and not driven by large-scale fluctuations, while TSAS was significant.

While more recent studies did not confirm TSAS abundance and properties claimed by Frail et al., and have questioned spectrometer accuracy (Stanimirovic et al. 2010) and statistical significance of some of their detections (Johnston et al. 2003), the Frail et al. study provided an important impetus for future experimental and theoretical work.

**2.2.2. More Recent Studies.** The recent era of sensitive pulsar TSAS experiments began with the Parkes observations of Johnston et al. (2003). These investigators found no significant optical depth variations in their three-epoch observations of three pulsars (0736-40, 1451-68 and 1641-45, for limits see Table 1). In comparing their work with previous studies, they showed that Frail et al. (1994) did not fully account for the large increase in noise in absorption spectra at the line frequency, suggesting that some of Frail et al. detections were not real. They found TSAS only in the case of one pulsar: PSR B1557-50. This is the same pulsar whose HI spectral variability was noted earlier by Deshpande et al. (1992). In combining the results from four measurements over twenty-five years, Johnston et al. (2003) found a TSAS feature  $\sim 1000$  AU in size, with  $n_H \sim 10^4$  cm<sup>-3</sup>. They explained their detections and non-detections as agreeing with the Deshpande (2000) picture.

Minter, Balser & Kartaltepe (2005) performed a comprehensive TSAS search in the direction of PSR B0329+54 with the Green Bank Telescope. The pulsar was observed in eighteen sessions over a period of 1.3 yr, yet no HI optical depth variations were detected for pulsar transverse offsets ranging from 0.005–25 AU<sup>6</sup>. This study also tested the Gwinn (2001) explanation of small-scale structure as being due to a combination of interstellar scintillation and gradients in the Doppler velocity of HI but did not find support for this model. While no HI optical depth variations were observed, Shishov et al. (2003) have obtained diffractive scintillation measurements for this pulsar. They found that below 2000 AU the diffractive scintillation can be explained with a scattering screen comprised solely of ionized gas. On scales larger than 2000 AU their results require some neutral gas to be present inside the scattering screen. Minter et al. suggested that therefore the inner scale of neutral gas could be around 2000 AU and that this could

<sup>6</sup>For consistency we normalized scales to assume that absorbing material is at the position of the pulsar which is a common assumption for many studies.

explain the lack of HI absorption variability below 2000 AU.

In their HI absorption study of pulsars in the first Galactic quadrant, Weisberg et al. (2008) noticed that one of three pulsars with previous HI absorption measurements, PSR B0301+19, exhibited significant changes in its absorption spectrum over a period of 22 yr, indicating TSAS on a 500 AU scale.

**2.2.3. Variability in the direction of B1929+10 and the ubiquity of TSAS.** A new multi-epoch pulsar experiment re-observed Frail et al. (1994) targets at even higher sensitivity (Stanimirović et al. 2003; Weisberg & Stanimirović 2007; Stanimirović et al. 2010). B0540+23 was excluded from the analysis due to strong interstellar scintillation causing complex baseline ripples. TSAS was detected only in the case of B1929+10 and only for the strongest of its three velocity components (shown in Figure 5), when considering both equivalent width of the HI optical depth and difference spectra between two epochs. Table 2 lists information for all pulsar detections and non-detections. Four detected TSAS features have a size of 6–40 AU,  $N(HI) = (1 - 3) \times 10^{19} \text{ cm}^{-2}$ ,  $n_H > 10^4 \text{ cm}^{-3}$  (assuming spherical geometry) and  $P/k > \text{a few} \times 10^6 \text{ cm}^{-3} \text{ K}$ . The fraction of HI associated with TSAS was found to range from 0% to 11%, with a median value of 4%. In addition, by combining their measurements and upper limits with published results, Stanimirović et al. (2010) found that the maximum detected  $\Delta\tau$  showed an increasing trend with the peak optical depth.

Stanimirovic et al. (2010) found that derived  $T_s = 150 - 200 \text{ K}$  for HI components in the direction of B1929+10 are significantly warmer than what is typically found for the CNM (e.g. 20-70 K). In addition, this line of sight has only 7% CNM fraction of the total neutral gas, while other sightlines have 15-20%. B1929+10 has a distance of only  $361_{-10}^{+8} \text{ pc}$  and is the closest in the observed sample with one half of its line of sight being inside the Local Bubble, running along the Local Bubble wall for  $\sim 50 - 60 \text{ pc}$ . Based on a comparison with Na I observations, it is likely that the absorbing clouds traced via varying optical depth are at a distance of  $< 106 \text{ pc}$  (Genova et al. 1997), confirming their association with the Local Bubble, in support of the measured high  $T_s$ .

The examination of all pulsar and interferometric TSAS detections and upper limits by Stanimirović et al. (2010) did not show a correlation between the level of optical depth fluctuations and the TSAS spatial scale, as would be expected if the turbulent spectrum on much larger scales is extrapolated to AU-scales. The detections and non-detections probed an almost continuous range of spatial scales from  $\sim 0.1$  to 1000 AU. This study concluded that the large number of non-detections of TSAS suggests that the CNM clouds on scales  $10^{-1}$  to  $10^3 \text{ AU}$  are not a pervasive property of the ISM. The sporadic TSAS detections on scales of tens of AU could indicate an intermittent process that forms discrete structures or turbulence associated with large scale features (such as the Local Bubble Wall) rather than end-points of a universal turbulent spectrum.

Another striking result from their study was a possible correlation between B1929+10's TSAS and interstellar clouds observed in Na I absorption inside the Local Bubble. There is significant evidence that the TSAS in the direction of B1929+10 is likely to be within  $\sim 100 \text{ pc}$  of the Sun, and is sampling the small-scale structure of the Local Bubble likely caused by hydrodynamic instabilities fragmenting the Local Bubble wall. Stanimirovic et al. (2010) proposed that the line of sight of B1929+10 is revealing this recently formed TSAS. Similar bubbles and their walls are found throughout the Milky Way, but the lifetime of a TSAS cloud created from them depends strongly on the its size and the temperature of the surrounding medium. Larger fragments (size  $\sim 10^4 \text{ AU}$ ) survive longer and can travel large ISM distances, becoming a more general ISM property. On the other hand, the smallest clouds (size  $\sim 10 - 100 \text{ AU}$ ) evaporate quickly close to their formation site, and are therefore not very commonly observed in the ISM. Additional processes, such as stellar mass-loss and collisions of interstellar clouds/filaments, could also contribute to the CNM structure formation on somewhat larger (sub-pc) scales.

In summary, the preponderance of evidence in recent years (and increased sensitivity of radio instruments) suggests that TSAS is *not* ubiquitous. What physical and environmental conditions, and spatial scales are more conducive for TSAS formation and evolution is still not clear. While several pulsar measurements detected TSAS on spatial scales of  $\sim 10 \text{ AU}$ , in one direction (B0329+54) it was suggested that the inner scale of TSAS is more likely to be 2000 AU. There is significant evidence that TSAS in the direction of B1929+10 is within the Local Bubble and likely associated with the fragmenting Local Bubble wall.

### 2.3. Spatial and temporal variability of optical and ultraviolet lines

Several different methods have been employed to study TSAS using optical and ultraviolet transitions. Spatial variability of line profiles in the direction of stars in binary and multiple stellar systems typically probes spatial scales of a few thousands of AU. With modern multi-object spectrographs, even 2D images of the absorbing medium can be reproduced using hundreds of stars in globular and open clusters. In addition, temporal variability of absorption

lines against stars probes even smaller spatial scales of  $\sim 1$  to tens of AUs, Figure 1.

The most commonly used transitions for such studies are Na I lines at 5889 and 5895 Å due to their strengths and availability from the ground, relatively high gas phase abundance, as well as the wavelengths being at the peak of efficiency of high-resolution spectrographs (Lauroesch 2007). Other commonly used species are Ca I, Ca II, K I, and even molecular lines like CH and CN. In more recent years, several studies have observed the diffuse interstellar bands (DIBs) – over 400 broad optical absorption features in the 4000-9000 Å range whose origin is still debated but are likely produced by carbonaceous molecules. In addition, many UV lines, from dominant ions such as Mg I, Cr II, Zn II, S II, are available using space-based observations and can provide useful diagnostics via line ratios.

The key difference between radio and optical observations of TSAS is that lines in the optical come mainly from trace ionization states (Na I, K I) and elements which are highly depleted onto dust grains even in diffuse clouds. This makes the interpretation of optical variability very complex as line profile variations can reflect changes in the column density, but also variations in the physical conditions (such as density, ionization history, temperature, or even chemistry). In our summary of main results from optical/UV observations of TSAS we follow somewhat an excellent review provided by Lauroesch (2007).

**2.3.1. Early Studies.** The very first studies to note variations in the optical line profiles over small angular scales go back all the way to Münch (1953) and Münch (1957). The binary stars observations by Meyer (1990, 1994) found variability of Ca II absorption lines with a higher frequency on scales larger than 2500 AU. Using the Anglo-Australian Telescope Meyer & Blades (1996) observed five binary pairs and found Na I variability in all cases on spatial scales of 2800–12,300 AU. Especially striking were two stars in  $\mu$  Cru, separated by 6600 AU<sup>7</sup>, where the component at 5 km/s has changed in column density by  $2 \times 10^{11}$  cm<sup>-2</sup>. Although Na I is not a dominant ion in HI clouds, an empirical relation exists between  $N(\text{NaI})$  and  $N(\text{H})$ . This relation implied a change in the H column density of  $N(\text{H}) > 10^{20}$  cm<sup>-2</sup> and the TSAS number density of  $n_{\text{H}} > 10^3$  cm<sup>-3</sup>. It has been known, however, that the  $\mu$  Cru sightline passes through an expanding shell associated with Loop I. Building further statistics, Watson & Meyer (1996) studied 15 binary and two triple systems covering projected separations of 480 to 29,000 AU and found significant variations for all systems. However, they also found several cases where variability was occurring for some, but not all, velocity components. Similarly to early radio observations of TSAS, they concluded that TSAS traced by Na I is likely ubiquitous.

Lauroesch & Meyer (2003) observed temporal variability over a period of 8 years toward  $\rho$  Leo using Na I and Ca II transitions. They found that the velocity component at 18 km/s showed significant temporal variability in Na I on scales of  $\sim 12$  AU, however Ca II stayed unchanged. This prompted them to use archival Hubble Space Telescope (HST) observations of other species to measure thermal pressure of  $P/k < 10^{3.3-3.8}$  cm<sup>-3</sup> K and  $n_{\text{H}} < 20$  cm<sup>-3</sup> using C I lines. These results, both for pressure and density, are significantly lower than what is traditionally assumed for the overpressured models of TSAS. Furthermore, the Cr II to Zn II ratio and the estimated electron density all suggested properties typical for diffuse clouds. This study clearly highlighted complications when dealing with Na I - the Na I column density changes in this particular direction were clearly driven by changes in physical conditions of the absorbing gas, not the total gas column density, which would happen in the presence of discrete structures. They suggested a picture where the bulk of trace species are in density peaks so their patchy distribution gives an appearance of large fluctuations on AU scales. Similar results were obtained in other studies. For example, Lauroesch et al. (1998) used HST observations to show that for  $\mu$  Cru common neutral species show variations, while dominant ions do not. Further studies by Lauroesch & Meyer (1999); Pan, Federman & Welty (2001); Welty (2007) especially argued for density variations and/or ionization variations within larger interstellar clouds as being the cause of observed column density differences.

More recent studies have employed even higher spectral resolution multi-object and integral-field spectrographs (e.g. WIYN's DensePak) to map Na I absorption in the direction of many stars, providing essentially 2-D images of the absorbing medium towards globular clusters M 15 and M 92 (Meyer & Lauroesch 1999; Andrews, Meyer & Lauroesch 2001) and open clusters  $h$  and  $\chi$  Per by Points, Lauroesch & Meyer (2004). Complex and significant variations are often found down to spatial scales of 70,000 AU.

While spatial variability of optical profiles is common, the number of stars that have shown temporal variability is relatively small. For example, Lauroesch & Meyer (2002) found that only  $\sim 15\%$  of stars in their sample showed temporal variability. In several directions with observed temporal variability densities of 20–200 cm<sup>-3</sup> were estimated, again signaling complex underlying physical conditions instead of changes in the total column density that could be

---

<sup>7</sup>A distance of 170 pc was used in this study.



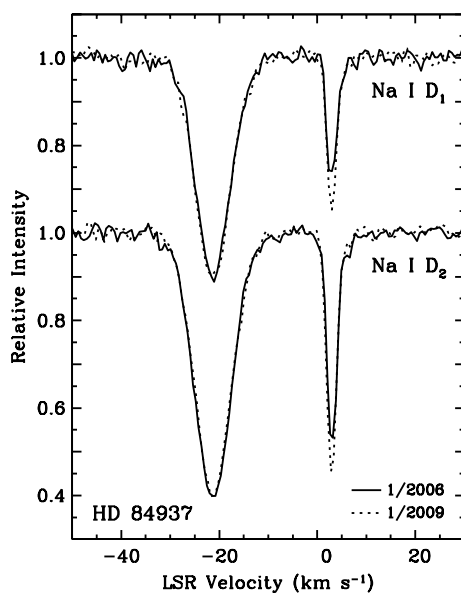


**Figure 6**

Comparison of the Na I D absorption profiles toward HD 84937 in KPNO coude feed spectra taken in 2006 January and in 2009 January. While the broader stellar Na I absorption at  $21 \text{ km s}^{-1}$  is identical in both spectra, the narrow LLCC Na I absorption exhibits a significant difference in strength between the two epochs. From Meyer et al. 2012.

caused by a passage of a discrete interstellar cloud. In addition, most temporal variations were observed in trace species and the majority of sightlines were behind supernova remnants (SNRs) or HI shells.

**2.3.2. Studies with larger samples.** More recent studies of TSAS have focused on expanding sample size, as well as observing multiple ionization species so that electron density and the total hydrogen number density can be estimated. Following Danks et al. (2001) who studied 10 stars and Smoker et al. (2011) who studied 46 sightlines (with only 3 showing temporal variability), McEvoy et al. (2015) represents the largest sample of stars searched for absorption variability over two epochs. 104 stars in total were studied over periods 5-20 years (covering a range of spatial scales of a few to  $\sim 200 \text{ AU}$ ). However, only 6% of stars showed variability in Na I, Ca I or Ca II. The study concluded that while less common at  $< 360 \text{ AU}$ , TSAS could be still ubiquitous on scales  $> 480 \text{ AU}$ . By assuming Ca ionization equilibrium, a temperature of 100 K, and that Ca I and Ca II sample the same line of sight, they estimated  $n_e$ , and then  $n_H$ . All sightlines with detected variability (6% of the total sample) have been found to have  $n_H > 1000 \text{ cm}^{-3}$ , in agreement with typical TSAS structures. While the Ca ionization equilibrium is a promising technique for estimating  $n_e$ , and confirming TSAS based on  $n_H$ , this study found  $n_e = 0.2 - 0.6 \text{ cm}^{-3}$  which is higher than typical estimates from other dominant species. In addition, several previous studies have shown that Ca estimates of  $n_e$  appear to be significantly overestimated. This is a concern and likely suggests that assumptions used in the Ca ionization equilibrium calculations need to be revisited. As we summarize in the next section, many cases of optical variability have been found close to SNRs or expanding shells. As these are highly dynamic regions, often dominated by shock chemistry, the assumptions of photoionization equilibrium may not be appropriate.

An even larger sample of 800 sightlines was obtained by van Loon et al. (2013). These authors used the Very Large Telescope to observe stars in the direction of 30 Doradus in the Large Magellanic Cloud, focusing on 4428 and  $6614 \text{ \AA}$  DIB features, as well as Na I and covering both LMC and Galactic velocities. While the origin of DIBs is still not known, it is accepted that they trace diffuse ISM (Herbig 1993; van Loon et al. 2013). By looking at the difference between pairs of Na I spectra, van Loon et al. (2013) noticed significant variations that gradually increase over the spatial scales probed, 2000 to 35,000 AU, assuming that Galactic absorbing gas is at a distance of 100 pc.

In summary, most recent optical studies, with larger samples and direct estimates of the TSAS density, suggest that only a few percent of sightlines exhibit TSAS-tracing variability.

**2.3.3. TSAS observations in the direction of supernova remnants.** Since early days optical TSAS examples were occasionally found in the direction of SNRs and many studies have specifically searched for optical variability towards sources within and in the vicinity of supernova remnants. In particular, Vela has been extensively studied (Hobbs et al. 1991; Danks & Sembach 1995; Cha & Sembach 2000; Welty, Simon & Hobbs 2008) and several exceptional cases of optical variability have been discovered.

More recently, Rao et al. (2016) studied Na DI spectra of 64 OB stars in the direction of Vela and made a temporal comparison with earlier observations by Cha & Sembach (2000). For three of the stars that showed major decrease in the low-velocity absorption, Kameswara Rao et al. (2017) obtained also SALT Ca II K absorption spectra and found lack of variability. While it is still puzzling how can Na I and Ca II profiles be so different, this study suggests that shocks associated with the SNR could be destroying local clouds and causing optical variability. Similarly, Dirks & Meyer (2016) studied HD47240, a star located behind the Monoceros Loop SNR over a period of 8 years, probing angular separations of  $\sim 10$  AU. They found dramatic changes in Na I profiles and even a splitting of one velocity component, and concluded that such drastic variability is related to local phenomena. and likely not a pervasive component of the ISM.

Time variability toward  $\kappa$  Velorum was studied in Smith et al. (2013) and a continuous increase in the equivalent width and column density of Ca I and K I lines was found on scales 5-25 AU, but not in several other species. With estimated depletion pattern and electron density they calculated  $n_H > 7 \times 10^3$  and  $2 \times 10^4 \text{ cm}^{-3}$ . Based on distance constraints, it is likely that the absorbing clouds are located just beyond the edge of the Local Bubble.

Meyer et al. (2012) studied the Local Leo Cold Cloud (LLCC) located inside the Local Bubble and at a distance 11–24 pc. Using C I lines, they measured very high thermal pressure of  $P/k \sim 6 \times 10^4 \text{ K cm}^{-3}$ . With an estimated temperature of 20 K and the HI column density of  $10^{19} \text{ cm}^{-2}$ , these observations implied  $n_H \sim 3000 \text{ cm}^{-3}$  and a line-of-sight thickness of 200 AU. Multi-epoch Na I observations in the direction of several stars found evidence for 46-AU structure in the direction of one star, while no change in several stars which have much smaller proper motion. They suggested that such small, over-dense TSAS clouds inside the Local Bubble could be formed at a collision interface between flows of warm clouds.

In summary, many optical studies have suggested a possible connection between SNRs and TSAS traced by optical observations, e.g. Crawford (2003). Meyer, Dirks & Lauroesch (2015) found Na I variations in 12/20 sightlines with all cases being associated with SNRs or stellar bow shocks. These results suggest that physical processes associated with shock propagations and SNR evolution are important for TSAS formation and survival. This conclusion agrees with Stanimirovic et al. (2010) who found persistent HI optical depth variability in the case of PSR B1929+10, which is likely tracing TSAS formed in fragmentation of the Local Bubble wall. Motivated by the theory of evaporation of cold clouds in a *hot* medium (Cowie 1975; Cowie & McKee 1977), Stanimirovic et al. (2010) suggested that while similar fragmentation events occur frequently throughout the ISM, the warm medium surrounding these cold cloudlets induces a natural selection effect wherein small TSAS clouds evaporate quickly and are rare, while large clouds survive longer and become a general property of the ISM. This is discussed further in §2.4.

## 2.4. Theory of Neutral Structures

The main issues in the theory of TSAS are how structure forms on such small scales, whether the structures are as highly overpressured as implied by simple analysis, and whether they are in equilibrium or highly transient. Addressing these issues requires accounting for a wide range of physical processes including turbulent flows, magnetic fields, radiative and conductive cooling, ion-neutral friction, and possibly self gravity. In addition, for both electrons and atomic tracers there is continuing debate over whether TSAS and TSIS exist throughout the ISM or whether they are produced primarily in “special” locations such as shocks and shells. Whether the sites of TSAS and TSIS are physically associated is an open question that could be addressed by better statistics and coordinated measurements.

In this section, we first consider the possibility that TSAS could be related to interstellar turbulence, and then consider implications for TSAS if it is in the form of tiny clouds.

**2.4.1. Interpretation of optical depth statistics.** An alternative to the picture of TSAS as tiny overpressured cloudlets was presented in Deshpande, Dwarakanath & Goss (2000) and is based on the analysis of HI optical depth statistics discussed in §2.1.4.

Spatial variation of optical depth  $\tau(\mathbf{x})$  can be quantified by the structure function:

$$S(\Delta\mathbf{x}) = \langle |\tau(\mathbf{x}) - \tau(\mathbf{x} + \Delta\mathbf{x})|^2 \rangle. \quad (2)$$

If  $S(\Delta\mathbf{x})$  is a power law,  $S(\Delta\mathbf{x}) \propto |\Delta\mathbf{x}|^\alpha$ , then, from Lee & Jokipii (1975), the optical depth variation  $\Delta\tau(\Delta\mathbf{x})$

should scale as  $(\Delta x)^{(\alpha-2)/2}$ . For  $\alpha = 2.75$ , the value measured for Cas A (Deshpande, Dwarakanath & Goss 2000),  $\Delta\tau(\Delta x) \propto \Delta x^{0.38}$ . This means that blotchy optical depth at large scales translates to significant opacity variations at small scales. An oversimplified but suggestive way to visualize this is to imagine looking through a set of large, semitransparent disks suspended randomly in space against an illuminated background. There will be some closely spaced pairs sightlines that pass through different numbers of disks and therefore see different levels of brightness. However, this small scale variation is produced by structures much larger than the separations of the sightlines.

Thus, Deshpande (2000) argues that the observed small scale variations in  $\tau$  do not require tiny, overdense, overpressured clouds. Rather, the observed optical depth differences are consistent with a single power-law description of the HI optical depth distribution as a function of spatial scale. The observed variations in optical depth sample the square-root of the structure function of the HI optical depth, not directly the power spectrum of optical depth fluctuations. This is a key point. As to why the autocorrelation of the HI optical depth should have the power law property, and what controls  $\alpha$  we turn to theories of turbulence.

**2.4.2. Turbulence in the neutral ISM.** Turbulence in neutral gas can produce small scale structure in two different ways. Interstellar turbulence, being transonic or mildly supersonic, is compressible. Density fluctuations are a natural part of compressible turbulence, and, if the turbulence is subsonic or transonic, have a spectrum similar to the energy spectrum (§1.3). The only question is whether compressible turbulence can persist to AU scales, or becomes noncompressive or dissipates on larger scales. Small scale density fluctuations are also generated from large scale density gradients by chaotic fluid motions, which bring previously widely separated fluid elements, with very different densities, into close proximity.

Turbulence in the CNM is both magnetized and weakly ionized. Magnetized turbulence in weakly ionized gas is discussed in Cho, Lazarian & Vishniac (2002); Cho & Lazarian (2003); Li, McKee & Klein (2006); Inoue & Inutsuka (2008); Tilley & Balsara (2011); Burkhart et al. (2015); Zweibel (2015). The magnetic field acts directly only on the plasma, which transmits magnetic forces to the neutrals through collisions on a timescale  $\tau_{ni} \equiv \nu_{ni}^{-1} \sim 5.3 \times 10^8/n_i$  s (Draine, Roberge & Dalgarno 1983) for an ion number density  $n_i$  and ions more massive than neutrals. If  $\tau_{ni}$  is short compared with the characteristic dynamical time  $\tau_{dyn}$ , the plasma and the neutrals move together as a single, magnetized fluid, while for  $\tau_{ni}/\tau_{dyn} < 1$ , they decouple. For processes on scale  $L$  we define  $\tau_{dyn} \equiv (L/v_A)(1+M_A)^{-1}$ , where  $v_A \equiv B/\sqrt{4\pi\rho} = 2.0 \times 10^5 B_\mu/n_n^{1/2}$  is the Alfvén speed in  $\text{cm s}^{-1}$ ,  $B_\mu$  is magnetic field strength in  $\mu\text{G}$ ,  $n_n$  is the neutral number density, and  $M_A \equiv v(L)/v_A$  is the Alfvén Mach number defined with respect to the typical velocity at scale  $L$ . We then define the decoupling scale  $L_d$  as the scale at which  $\tau_{dyn} = \tau_{ni}$ :

$$L_d \equiv \frac{v_A \tau_{ni}}{1 + M_A} \sim 1.1 \times 10^{14} \frac{B_\mu}{n_n^{1/2} n_i (M_A + 1)} \text{cm}. \quad (3)$$

$L_d$  is the scale below which the magnetic field and plasma slip through the neutral fluid in less than the flow time. Equation 3 agrees with the criteria given by Klessen, Heitsch & Mac Low (2000), Zweibel (2002). This is also the scale at which the ambipolar Reynolds number  $R_{AD}$  defined in Zweibel & Brandenburg (1997) is of order unity. In the cold, neutral ISM,  $L_d$  is typically a few tens to hundreds of AU.

At scales below  $L_d$  the plasma and neutrals follow different dynamics. The plasma develops an independent cascade with many current sheets and associated electron density filaments that if sufficiently dense could be an important source of interstellar scintillation. The neutrals evolve independently of the plasma and magnetic field. Since  $L_d$  is generally much less than the outer scale of turbulence, the hydrodynamic cascade shortward of  $L_d$  is expected to be quite subsonic and therefore incompressible. Density fluctuations become large only if the medium is nearly thermally unstable, in which case large, early isobaric density fluctuations could occur (Hennebelle & Audit 2007). However, a calculation with a large dynamic range and all physical processes accounted for is still lacking. Notably, however, the slope of the power spectrum of the optical depth autocorrelation function is close to the prediction of Lazarian & Pogosyan (2004) for optically thick media.

Large pressure fluctuations are possible in a turbulent medium; they tend to be associated with large velocity fluctuations. As a rough guess, we estimate that to confine a structure that is overpressured by a factor of 100, a turbulent velocity at least 10 times the rms velocity is required (McKee & Zweibel 1992). If the velocity probability density function (PDF) is Gaussian, the probability of creating such a velocity is exponentially small, but if the turbulent velocity PDF has a power law tail the fraction of power at high velocities is larger. For example, Falkovich & Lebedev (1997) suggested that the velocity PDF has the form  $(v/v_0)^{-4}$  for  $v/v_0 \gg 1$ . Non-Gaussian velocity PDFs could, for example, result from stellar winds, self-gravity, or even large-scale turbulent driving (Ossenkopf & Mac Low 2002). While density PDFs in turbulent flows have been studied by many authors, and velocity PDFs have been studied

for self gravitating turbulence (Klessen, Heitsch & Mac Low 2000), characterizing the velocity and pressure PDFs at small scales, including cooling, is an important problem for the future. On the observational side, better statistics on the line of sight and covering factor distributions would tighten the constraints on turbulence models of pressure fluctuations.

**2.4.3. Tiny neutral clouds.** Having considered the possibility that observations of TSAS could be explained by a power spectrum of opacity variations, and discussed their relationship to interstellar turbulence, we now discuss whether they could, in fact, be tiny clouds, as proposed originally. If the clouds are spherical, they must be highly overpressured. In §1.2, we estimated the energy input to the ISM resulting from free expansion of tiny overpressured clouds, and argued that this sets an upper limit on the filling factor of such clouds. The overpressure problem is less extreme for elongated clouds viewed end on, and we account for this in discussing gravitational and magnetic confinement.

**Thermal equilibrium.** We assume the clouds are heated by photoelectrons from dust, as in the rest of the CNM. Then, from Wolfire et al. (2003), especially Figures 8 and 11, we see that it is possible to maintain thermal equilibrium for high densities and low temperatures, e.g.  $n_H \sim 10^3 \text{ cm}^{-3}$ ,  $T \sim 30 \text{ K}$ , similar to what was derived for the Local Leo Cold Cloud (Meyer et al. 2012) and warmer than proposed in Heiles (1997), which invoked cooling by molecular species as well as by the C II 158 $\mu\text{m}$  line, which normally dominates CNM cooling. The resulting pressures are still high, and so in the absence of a confinement mechanism the clouds will expand.

Assuming that the C II fine structure line is the main source of radiative cooling, the radiative loss function is (Spitzer 1978)  $\Lambda = 7.9 \times 10^{-27} d_C e^{-92/T} \text{ cm}^3 \text{ s}^{-1}$ , where  $d_C$  is the carbon depletion factor. The result agrees with the fitting formula in Wolfire et al. (2003) to 20% at 100 K if we take  $d_C = 0.35$  to match the gas phase C abundance they assumed, and can be extrapolated to lower temperatures. Estimating the dynamical time  $t_{dyn}$  as  $R/c_s$ , where  $c_s \equiv \sqrt{kT/m}$  and the cooling time  $t_{cool} \equiv 3kT/2n\Lambda$  we define the minimum column density  $N_{min,c}$  such that  $t_{dyn}/t_{cool} > 1$ :

$$N_{min,c} = 1.2 \times 10^{15} T^{3/2} e^{92/T} \text{ cm}^{-2}. \quad (4)$$

For  $T = 50 \text{ K}$ , eqn. (4) gives  $2.7 \times 10^{18} \text{ cm}^{-2}$ , which is in the range for TSAS (see Tables 1 and 2). We might expect clouds with  $N \ll N_{min,c}$  to expand (and cool) adiabatically. Clouds with  $N \gg N_{min,c}$  would cool radiatively faster than they expand and might then reach a thermal equilibrium - which is still overpressured.

**Gravitational confinement.** Overpressured clouds can maintain equilibrium if they are gravitationally or magnetically confined. For a given column density, self gravity is less effective relative to external pressure in confining a prolate cloud than a spherical cloud. It can be shown from the virial theorem, using expressions in Bertoldi & McKee (1992), that the ratio of the external pressure confinement term to the gravitational confinement term  $X_c$  is:

$$X_c = \frac{15P_s}{\pi GN^2 m_H^2} \frac{y\sqrt{y^2-1}}{\ln\left(y + \sqrt{y^2-1}\right)}, \quad (5)$$

where  $N$  is the column density along the major axis,  $P_s$  is the surface pressure, and  $y$  is the ratio of major to minor axis. Equation (5) shows that gravitational confinement of highly elongated clouds ( $y \gg 1$ ) is much less effective relative to pressure confinement than it is for spherical clouds ( $y = 1$ ). For example, if  $y = 10$ ,  $X_c$  is about 33 times larger than for a spherical cloud. Therefore, filamentary clouds must be very close to pressure balance with their environments, even accounting for self gravity.

**Magnetic confinement.** Overpressured filamentary clouds can maintain equilibrium if they are magnetically confined. Many configurations are possible (Fiege & Pudritz 2000), but here we consider the simple case of a filamentary cloud of radius  $R$  with internal pressure  $P(r)$  confined by a helical magnetic field  $\mathbf{B} = B_z \hat{z} + B_\phi(r) \hat{\phi}$ , with  $B_z$  a constant. The magnetic force points radially inward if  $rB_\phi$  is an increasing function of  $r$ . It can be shown from the virial theorem that the mean internal cloud pressure  $\langle P \rangle$ , external pressure at the cloud surface  $P_s$ , and azimuthal magnetic field component at the cloud edge  $B_\phi(R)$  are related by:

$$\langle P \rangle = P_s + \frac{B_\phi^2(R)}{8\pi}. \quad (6)$$

(The axial component  $\hat{z}B_z$  drops out because it is the same inside and outside the cloud). If  $P_s$  is of order the ambient ISM pressure, then the pressure in  $B_\phi(R)$  must be comparable to the TSAS pressure. For example, assume  $B_\phi = B_0 r/R$  for  $r < R$  and  $B_\phi = B_0 R/r$  for  $r > R$ . In order to satisfy force balance,  $P = P_c - B_0^2 r^2/(4\pi R^2)$  for  $r < R$  and  $P = P_c - B_0^2/4\pi$  for  $r > R$ . The ratio of surface pressure  $P_s = P_c - B_0^2/4\pi$  to central pressure  $P_c$  is

$1 - B_0^2/4\pi P_c$ , which is small only when  $B_0^2$  is slightly less than  $4\pi P_c$ . A magnetic field of  $10\mu\text{G}$  (about twice the rms galactic field; Zweibel & Heiles (1997)) would support a central pressure  $P_c/k = 5.8 \times 10^4 \text{ K cm}^{-3}$ .

A cloud can only be magnetically confined for as long as it takes the magnetic field and plasma component to drift through the neutral component, which comprises most of the mass. In the situation described here, the magnetic field and plasma drift inward, which allows the neutral component to drift outward. From §2.4.2 (see eqn. (3)), and assuming rough equality of gas and magnetic pressure, we can write the ratio of the drift speed  $v_D$  to the expansion speed  $c_S$  as:

$$\frac{v_D}{c_S} \sim \frac{c_S \tau_{ni}}{R} \sim \frac{\tau_{ni}}{\tau_{dyn}} \sim 3.5 \frac{v_5}{n_i R_{AU}}, \quad (7)$$

where  $v_5$  and  $R_{AU}$  are the sound speed and radius in km/s and AU, respectively. Equation (7) says that the cloud can be confined for more than its free expansion time if the neutral-ion collision time is short compared to the dynamical time, and sets a lower limit on the radius of a magnetically confined filament. For example, if  $n_i = 0.1 \text{ cm}^{-3}$  (ionization fraction of  $10^{-4}$  with  $n = 10^3 \text{ cm}^{-3}$ ) and  $v_5 = 1 \text{ km/s}$ , then  $v_D/c_S < 1$  for  $R > 35 \text{ AU}$ . The similarity of this scale to TSAS suggests that there is a critical width below which filaments cannot be magnetically confined, whereas for larger TSAS, magnetic confinement is possible for quite long times. The filamentary morphology is potentially attractive for explaining thin H I fibers (Clark, Peek & Putman 2014; Kalberla & Kerp 2016).

**Thermal conduction.** As noted by Heiles (1997), the overpressure problem is reduced if TSAS is colder than the surrounding CNM. Heat will then flow into the cloud, which will either shrink due to evaporation or grow due to condensation, depending on whether the column density is below (evaporation) or above (condensation) a critical column density  $N_c$  at which radiation and conduction balance (McKee & Cowie 1977). Balancing the conductive heating and radiative cooling terms in the energy equation yields (Inoue, Inutsuka & Koyama 2006):

$$N_c = \left( \frac{\kappa T}{\Lambda} \right)^{1/2}, \quad (8)$$

where  $\kappa$  and  $\Lambda$  are the thermal conductivity and radiative loss function, respectively. For the CNM we take  $\kappa = 2.5 \times 10^5 T^{1/2} \text{ erg s}^{-1} \text{ K}^{-1} \text{ cm}^{-1}$  and  $\Lambda = 2.8 \times 10^{-27} e^{-92/T} \text{ cm}^3 \text{ s}^{-1}$ , corresponding to C II cooling with a gas phase Carbon abundance of  $1.4 \times 10^{-4}$ . Substituting these expressions into eqn. (8) and normalizing  $T$  to 30 K gives  $N_c = 5.6 \times 10^{17} T_{30}^{3/4} e^{1.53/T_{30}} \text{ cm}^{-2}$ , which is compatible with column density measurements for TSAS.

Clouds with  $N \ll N_c$  will evaporate on a timescale  $\tau_{evap}$ :

$$\tau_{evap} \sim \frac{3nk_B R^2}{2\kappa} \sim 4.5 \times 10^{-9} \frac{NR_{AU}}{T_{30}^{1/2}}. \quad (9)$$

Clearly, conduction sets a lower limit on the thickness of a cold filament, which makes it difficult to maintain TSAS temperatures that are lower than other CNM temperatures and thus may explain why Brogan et al. (2005) found no difference between TSAS and other CNM temperatures. On the other hand, larger structures will grow as they accrete condensing material.

## 2.5. Summary and Outstanding Questions

**Ubiquity.** Spatial and temporal variability of different tracers, based on several different observational techniques, have found clear TSAS examples. However, as Tables 1 and 2 show, since early days TSAS was not seen in all observed directions. The preponderance of evidence is that TSAS is not ubiquitous in the ISM.

It is important to keep in mind that the three categories of observational techniques we discussed in this section, each have their own pros and cons, and often probe very different spatial scales (e.g. Figure 1). The interferometric imaging of  $\Delta\tau$  against extended background sources has a major advantage of providing spatial (and kinematic) 2D information about TSAS, and may even be able to constrain TSAS morphology in the future. Especially powerful are statistical measurements of the power spectrum of  $\Delta\tau$ . However, such measurements require exceptional sensitivity and are limited by the available source size, source surface brightness, and telescope resolution. Temporal variability of absorption profiles is more easily accessible observationally, yet suffers from one-dimensional sampling of the  $\Delta\tau$  distribution. As summarized in this section, some tension exists between results from two categories of radio measurements; while interferometric imaging of 3C138 and 3C147 claimed pervasive TSAS, temporal radio variability against pulsars and point-source extragalactic targets suggests that TSAS is not a pervasive component of the ISM. The later conclusion is in agreement with optical studies of TSAS where abundant evidence exists of TSAS associated with SNRs. Future high-cadence measurements are needed to resolve this tension. Brogan et al. (2005) questioned the ability to constrain the TSAS filling factor via temporal variability of absorption profiles as often a small number



(Zweibel 2005). This is also the range of scales at which the magnetic field, plasma, and neutrals transition from strongly to weakly coupled. In essence, the astrophysics on TSAS-scales is rich and exotic, and largely unexplored.

The turbulent power spectrum that exists in the ISM on larger scales is expected to continue below scales of hundreds of AU, however it becomes more complex as neutrals and ions split into different turbulent cascades. On theoretical grounds, we expect that the neutral turbulent spectrum at these scales becomes incompressible and has a Kolmogorov power spectrum slope. However, thermal instability can modify the turbulent cascade and enhance density fluctuations (Hennebelle, Audit & Miville-Deschênes 2007), while optical depth effects change the relationship between density and optical depth fluctuations, resulting in a shallower power spectrum of optical depth. Theoretically, therefore, TSAS could be part of the turbulent spectrum but observationally this is still not confirmed and it is not clear that density and pressure fluctuations of the required amplitude can be achieved by typical ISM turbulence. Mapping of HI absorption against three extended sources (Cas A, Cygnus A and 3C138) showed a similar power spectrum slope of 2.7 over a range  $\sim 10$  to 150 AU, and  $\sim 15,000$  AU to 3 pc. While this is impressive, we need to bridge the gap in the middle with future observations. In addition, the power spectrum amplitudes for different regions are different. The compilation of heterogeneous observations shown in Figure 7 (left) do not show a continuous spectrum. Therefore, we do not have evidence for a *continuous* power spectrum from few pc all the way to few AU.

Several physical processes place a lower limit on the cold TSAS cloud size of  $\sim 100$  AU. Thermal conduction suggests that smaller TSAS clouds would quickly evaporate, while magnetic field could not provide confinement for TSAS clouds smaller than  $\sim 100$  AU. All of this suggests that, theoretically, TSAS on scales  $< 100$  AU should be short-lived and transient, while larger TSAS clouds should be more frequent. Constraining observational abundance of small vs larger TSAS clouds could constrain these important physical processes.

Probing spatial scales of  $< 100$  AU observationally requires high resolution interferometric observations, and/or high sensitivity and frequent temporal sampling of absorption spectra (radio and optical). Several experiments have detected TSAS on spatial scales of few to 100 AU, e.g. Brogan et al. (2005); Stanimirović et al. (2010); Meyer et al. (2012), however more detections exist on scales  $> 100$  AU. While scales  $> 100$  AU are observationally easier to probe, and a higher frequency of TSAS could be driven by observational biases, the existing samples are very small and improving statistics is of high importance.

**What defines the level of observed optical depth variability?** While most sources showed  $\Delta\tau < 0.1$ , 3C138 and 3C147 stand out as sources that have shown a much higher level of variability measured persistently for over three decades in scale. In addition, several optical studies have noticed an increase in absorption line variability on large spatial scales (Meyer 1990, 1994; van Loon et al. 2013). If  $\Delta\tau$  is driven by interstellar turbulence, a power-law relation is expected between TSAS size and  $\Delta\tau$  as a consequence of the turbulence cascade from large to small scales. Based on the measured power-law of  $\Delta\tau$  in the case of Cas A, Deshpande (2000a) predicted  $\Delta\tau \propto l^{(\alpha-2)/2}$ , with  $\alpha = 2.75$  and  $\Delta\tau = 0.2 - 0.4$  on scales 50-100 AU. With larger statistical samples of TSAS we can start testing the predictions for both the slope and amplitude of the turbulent spectrum, as well as investigate possible correlations between  $\Delta\tau$  and other physical parameters (e.g. TSAS size, the total HI column density or the  $H_2$  fraction). Clearly, a lot more on this will come in the future with larger samples.

In Figure 7 we show the detected level of optical depth variations,  $\Delta\tau$ , from Tables 1 and 2, as a function of TSAS spatial scale (left) and the total line-of-sight HI column density (right). We use here only radio detections and omit optical observations due to the complexity associated with non-dominant ions. While  $\Delta\tau$  is a key observable obtained directly from optical depth profiles, we note that spectral velocity resolution varies among observations (we have listed this information in Tables 1 and 2). To compare all measurements we scaled  $\Delta\tau$  to the common velocity resolution of 7.3 km/s (this is the lowest velocity resolution in the sample). The total HI column density along lines of sight toward background sources was obtained either from individual references provided in the tables, or from the Arecibo Millennium (Heiles & Troland 2003) and 21-SPONGE HI absorption-line surveys (Murray et al. 2017, in prep) if this information was missing. These measurements include a correction for high optical depth. For a sub-sample of sources (3C147, 3C161, GRS1915, 3C405, PSR B1821+05, PSR B1557-50, PSR B0301+19) we did not have the full column density information and have obtained integrated HI column densities from the Effelsburg all-sky, HI emission survey (HI4PI Collaboration et al. 2016) by using the optically-thin limit. These are therefore lower limits of the HI column density.

The left figure is essentially a scatter plot, there is no obvious correlation between the observed optical depth variation and spatial scales for measurements sampling diverse interstellar directions. As discussed in Section 2.4, interstellar turbulence would result in a correlation between  $\Delta\tau$  and linear scale and for Cas A Deshpande (2000a) measured  $\Delta\tau \propto l^{0.38}$  (Roy et al. 2012 confirmed the same slope for 3C138 over the range of scales 5–100 AU). We overplot the predicted level of variations from Deshpande (2000a) in Figure 7 as a sloping line, with dashed lines

corresponding to  $\pm 2\text{-}\sigma$  slope uncertainties. As with observations, we have scaled the predicted  $\Delta\tau$  to correspond to a velocity resolution of 7.3 km/s. The lack of correlation in this plot may suggest that thermal conduction and/or magnetic field-gas decoupling are more important than turbulence in shaping the ISM structure on AU-scales. However, improving statistics is essential to understand processes at AU scales, especially by focusing on individual regions with a single set of physical parameters such as the energy input.

The right-hand figure appears more interesting as it suggests a rough correlation between  $\Delta\tau$  and the total HI column density. Galactic directions with higher column density appear to have higher level of  $\Delta\tau$  variations. This correlation follows the Galactic latitude trend: at  $|b| > 25\text{deg}$ ,  $N(\text{HI}) < 10^{21} \text{ cm}^{-2}$  and  $\Delta\tau \sim 0.02$ ; at  $5 < |b| < 10$ ,  $N(\text{HI}) = 10^{21-22} \text{ cm}^{-2}$  and  $\Delta\tau \sim 0.01 - 1$ ; at  $|b| < 5\text{deg}$ ,  $N(\text{HI}) > 10^{22} \text{ cm}^{-2}$  and  $\Delta\tau > 0.1$ . TSAS fluctuations appear larger at low latitudes. The increase of the HI column density at low latitudes is a consequence of the plane-parallel disk geometry, once column densities are corrected by a  $\sin(b)$  factor they stay roughly constant (Dickey & Lockman 1990). The increase of  $\Delta\tau$  with the column density is in agreement with Frail et al. (1994) and Stanimirović et al. (2010), who noticed that directions with high optical depth (and therefore high CNM column density) had higher level of  $\Delta\tau$  variations. TSAS seems to prefer lower Galactic latitudes and higher HI column density, similarly to the CNM,  $\text{H}_2$  and SNR distributions, again potentially signaling preferred formation sites. This correlation also suggests that TSAS detections are intimately associated with the larger scale structure of the parental HI clouds, and not a totally random phenomenon. In addition, as hinted by Stanimirović et al. (2010),  $\Delta\tau$  increases with  $\tau$  suggesting that the amplitude of density fluctuations is not universal as would be the case for universal interstellar turbulence. Instead, density fluctuations appear stronger at low Galactic latitudes and high HI column densities (and optical depths), consistent with the idea that excess energy injection occurs in such environments likely via supernova explosions.

**2.5.1. Outstanding Questions.** Several key questions concerning TSAS origin and properties remain open.

**Turbulent power spectrum and dissipation scales.** On the theoretical side, numerical simulations going all the way to dissipation scales and predicting the behavior of the power spectrum at such scales do not exist, and creating them would be a formidably computationally intensive task given the large range of space and time scales involved. Besides an empirically-driven power spectrum (based on Cas A, Cygnus A and 3C138 observations), we have no numerical/theoretical predictions for the level of  $\Delta\tau$  or column density variations that can be compared with observations. A related question concerns velocity PDFs. While density PDFs have been studied extensively numerically, very few studies of velocity PDFs exist. Characterizing velocity fluctuations, in theory and observations, is important as this can potentially drive pressure fluctuations. The anisotropy of fluctuations formed in this manner should be carefully investigated to assess whether anisotropic turbulence can create the H I fibers mentioned in §1.2 (Clark, Peek & Putman 2014; Kalberla & Kerp 2016).

The spectacularly similar power-spectrum slope for Cas A, Cygnus A and 3C138 covers spatial scales of  $\sim 10\text{-}150$  AU and  $\sim 15,000$  AU to 3 pc. This is almost six orders of magnitude but with a gap in the middle. These results are very exciting as they could be shaping “the Big Power Law in the Sky” but for the cold, absorbing medium, which could have large implications for TSAS and heating/cooling in the ISM. Filling the gap on scales 150–15,000 AUs is essential, as well as understanding the variations of the power spectrum amplitude across different regions. More interferometric mapping of extended radio sources is needed, using both SNRs and quasars. In addition, the two best studied extragalactic sources 3c138 and 3c147 both found TSAS only on spatial scales close to the resolution limit. Future observations are essential to confirm that this is not an observational artifact. Telescopes like MeerKAT will be able to test this against other SNRs.

As mentioned already, better statistics are essential to start making progress in understanding the origin and properties of TSAS. Existing observations span many observational techniques, each with its own systematics and limitations. Combining such diverse and small samples to search for global properties and trends is challenging. The related issue is inhomogeneous methodology used by different authors in estimating distance to the absorbing TSAS or spin temperature. Homogeneous samples could be achieved though frequent, long-term monitoring of sources (pulsars or extragalactic) with already detected TSAS. This would provide better sampling of individual lines of sight, enabling monitoring of individual TSAS features to see how they evolve with time. For example, pulsars with detected variability should be monitored to provide longer time baselines and test TSAS evolution (do certain directions show persistent TSAS, or does TSAS eventually disappear?).

**Formation mechanisms.** As an emerging trend points at supernovae as a potential common birth place of TSAS, detailed numerical simulations are needed with predictions for the TSAS spectrum and expectations for the frequency of TSAS away from birth places. It would also be worthwhile to isolate various critical processes in the



turbulent cascade, such as the evolution of entropy modes when cooling is included, ion-neutral decoupling, formation of vortex filaments that could wind up a magnetic field, and sites of enhanced magnetic dissipation (Zhdankin et al. 2013; Zhdankin, Uzdensky & Boldyrev 2015; Zhdankin, Boldyrev & Mason 2017). In addition, observational evidence that TSAS is less common away from SNRs is still lacking. Large-scale surveys could conclusively quantify TSAS abundance between localized regions and random ISM fields.

**TSAS environment and internal structure.** Long-term monitoring of directions with TSAS will enable studies of internal structure of TSAS. Observational constraints of TSAS spin temperature and magnetic field essentially do not exist and are key details for understanding TSAS over-pressure. For example, thermal conduction requires TSAS temperature to be similar to the CNM temperature. Similarly, theory suggests that larger TSAS can be easily magnetically confined with a magnetic field of order of  $10 \mu\text{m}$ . These are clear theoretical predictions that need to be confronted observationally. In addition, thermal equilibrium considerations suggest that TSAS clouds larger than  $\sim 100$  AU would cool radiatively. This would result in significant CII emission associated with TSAS that can be tested observationally.

At high TSAS densities it is possible to have various molecular species. This can be easily tested with the Atacama Large Millimeter Array (ALMA) observations of CO and other transitions by focusing on directions known TSAS. ALMA is also perfect for monitoring strong extragalactic sources and measuring molecular absorption from species like  $\text{HCO}^+$ , HCN, HNC etc which have been found in diffuse interstellar regions in the Milky Way (Liszt & Lucas 1996). Similarly, Hennebelle & Audit (2007) and Koyama & Inutsuka (2002) suggest that TSAS could be formed in shocked CNM. Observing shock tracers like SiO with ALMA can test this possibility.

In addition, broader observed velocity range can test more extreme origin theories “halo”. Most observations focus on high velocity resolution and do not have broad velocity coverage. Finally, the under- and over-pressure directions based on C I measurements by Jenkins & Tripp (2011) are fascinating and require further investigation.

### 3. Tiny Scale Ionized Structure

The warm ionized medium contains density fluctuations over a broad range of spatial scales which provide a unique imprint on propagating radio waves. Turbulent fluctuations in the plasma density and magnetic field cause stochastic spatial and temporal fluctuations in the refractive index in the ISM. As a result, radio waves propagating through a plasma medium experience variations. Due to scattering of radio waves the flux density of pulsars and other pointlike sources varies with time and frequency (interstellar scintillation), and angular size of radio sources increases due to the blurring effect of the turbulent medium. Through these effects, observations of pulsars and pointlike extragalactic sources have revealed a spectrum of plasma structures in the electron density distribution which follows a Kolmogorov spectrum over 5 or even 10 decades (Armstrong et al. 1995, Haverkorn & Spangler 2013). The inner scale of this turbulent cascade is 70-100 km (Rickett et al. 1995), while the outer scale reaches 4-30 pc. Diffractive scintillation effects produced by small scale structure decrease with increasing frequency while the opposite is true for refractive scintillation produced by larger scale structure (Rickett, Coles & Bourgois 1984). The outer scale seems to suggest the variance of density fluctuations  $\langle \delta n_e^2 \rangle^{1/2} \sim 10^{-3}$ . At a WIM temperature of 8000 K and electron density of  $\sim 0.3 \text{ cm}^{-3}$ , these tiny-scale density fluctuations do not pose the enormous overpressure problems of TSAS or the phenomena discussed below. While the Kolmogorov spectrum persists over several orders of magnitude, the line of sight distribution of the turbulent material is still not well understood (uniform filling factor or confinement to thin layers?). We return to this topic in § 3.2.

However, there are several observational phenomena that exhibit flux modulations and scattering angles that are much larger than what is expected for Kolmogorov turbulence. These involve: extreme scattering events, intra-day variability of flat-spectrum radio quasars, and parabolic arcs and arclets in pulsar “secondary” spectra. All these events are often referred to as “extreme scattering” and, assuming isotropy in shape (so the angular size on the plane of the sky can be combined with the column density to give volume density), require plasma pressures that are much greater than what is typical for the diffuse ISM. It is not known presently whether all these events are related or have a very different origin.

Extreme scattering events (ESE) are sources that show dramatic decrease (often  $> 50\%$ ) in the flux density at radio wavelengths, usually close to 1 GHz, and last for a period of several weeks to months. The flux density changes observed in ESEs are very different from the flickering of radio sources frequently observed at GHz frequencies and attributed to interstellar scintillation. While scintillation typically causes persistent variability on timescales measured in days and at a level of few percent (although larger flux changes are observed for “intra-hour” variability, which is thought to be produced by nearby scattering with systematic increasing wavelength), variability observed in ESEs is

much larger (often  $> 50\%$ ), smooth, lasts over several months, and does not have usually strong frequency dependence except near the wavelengths at which rays converge, forming caustics.

In addition, the flux density variability of radio sources has also been observed at a level of few to 10% and on timescales of 1-2 days. This was first noticed by Heeschen (1984) and Witzel et al. (1986), and is known as intraday variability (IDV). Since early days it was hypothesized that IDVs are caused by slow scintillation in the ISM and intergalactic medium. As summarized by Jauncey et al. (2016) and Bignall et al. (2015), the combination of time delay measurements, the discovery of  $\sim 10$  IDV sources that show an annual cycle in their variability, as well as a strong correlation with Galactic latitude; all overwhelmingly support the idea that interstellar scintillation is the primary cause of variability in IDVs. However, we emphasize that some events defy simple classification (e.g. Tuntsov et al. (2017)). As mentioned above, the spatial distribution and properties of the scintillation material are still not fully understood. Studies such as Cordes, Weisberg & Boriakoff (1985) and Lazio et al. (2008) suggest that scintillation results from localized regions, possibly even clumps, distributed throughout the Galactic disk. Given the many possible forms and distributions of interstellar density variations, and the possibly complex structure of the sources themselves, many forms of variation with time and frequency are evidently possible. As IDV sources have less extreme properties than ESEs and no, to an order of magnitude, overpressure problem (Heiles & Stinebring 2007; Tuntsov, Bignall & Walker 2013), we do not include them in this review.

Pulsar dynamic spectra (frequency vs time) have a characteristic pattern due to interstellar scintillation and their Fourier transform is called the secondary spectrum. Many sensitive observations have shown parabolic arcs in the secondary spectra, whose curvature depends on the location of the scattering material along the line of sight (Hill et al. 2005; Stinebring 2007). Arcs imply existence of many localized scattering screens along the line of sight, with properties in accord with the Kolmogorov turbulence and  $n_e$  typical for the ionized ISM. However, some observations have shown small sub-structure within scintillation arcs, called ‘‘arclets’’, which require small dense structures with a size of  $\sim 1$  AU,  $n_e \sim 100 \text{ cm}^{-3}$  and  $P/k \sim 10^6 \text{ K cm}^{-3}$  (Hill et al. 2005) to be explained.

This review focuses only on the most extreme TSIS: ESEs which have extreme over-pressure and over-density problems. While properties of scintillation arclets appear similar to those found in ESEs, and arclets have the over-pressure problem, we do not include them in this review. We also note that interplanetary scintillation causes even faster, on scales of seconds, flux density variability of compact radio sources and is caused by inhomogeneities in the ionized solar wind. A recent study of interplanetary scintillation using the Murchison Widefield Array (MWA) found evidence for structure on spatial scales from  $< 1000$  to  $10^6 \text{ km}$  ( $\sim 100 \text{ AU}$ ) (Kaplan et al. 2015).

### 3.1. Extreme Scattering Events

**3.1.1. Early Studies.** The first ESE event was discovered by Fiedler et al. (1987a). In their daily monitoring of 36 extragalactic sources using the Green Bank Interferometer over 7 years at 2.7 and 8.1 GHz, Fiedler et al. noticed unusual minima in the light curves of 7 sources. QSO 0954+658 (see Figure 8) showed exceptionally dramatic light curves with a minimum at 2.7 GHz being correlated with several sharp spikes at 8.1 GHz. Based on the coordinated behavior at the two frequencies without any time lags, intrinsic source variability was excluded as a possible cause of variability and it was concluded that variations are caused by an occultation event. The light travel time arguments suggested that the occulter is in the Milky Way with a transverse velocity  $< 300 \text{ km/sec}$ . Combined with the estimated proper motion from the rapid decline of the light curve, a distance of  $< 1.3 \text{ kpc}$  was implied. From the duration of the light curve minimum an estimate of the size of the occulter was provided,  $< 7 \text{ AU}$ . Trends at two frequencies suggested refractive effects through irregularities in the ionized gas density of the occulter. Assuming a spherical lens, the implied density of the occulter was  $n_e \sim 4 \times 10^4 \text{ cm}^{-3}$ , much greater than that of the diffuse ionized ISM. Fiedler et al. (1987) concluded that the occulting sources likely represent a new astrophysical phenomenon whose nature and stability need to be understood.

Romani, Blandford & Cordes (1987) provided a more detailed interpretation of the 0954+658 event and suggested that the high pressure in the refracting structures is naturally found inside old SNRs (or the edge of a Galactic outflow), proposing that SNRs could be natural sites for the plasma lensing sheets with the over-pressure lenses residing inside the high-pressure environment. They made an estimate that on average a line of sight will pass through about 100 face-on sheets. This will cause small scattering angles, however if the sheets have small density corrugations this can significantly increase the scattering angle.

Fiedler et al. (1994) summarized results from a monitoring of 40-150 sources over a period of 11 years with the Green Bank Interferometer, and 330 sources over a period of six months using the NRAO 300-foot radio telescope. Only 10 ESEs were detected in the 2.7 GHz light curves. While the original ESE in the direction of 0954+658 had counterparts at 8.1 GHz, most other ESEs only showed changes in flux density at 2.7 GHz. Also, a greater variety of

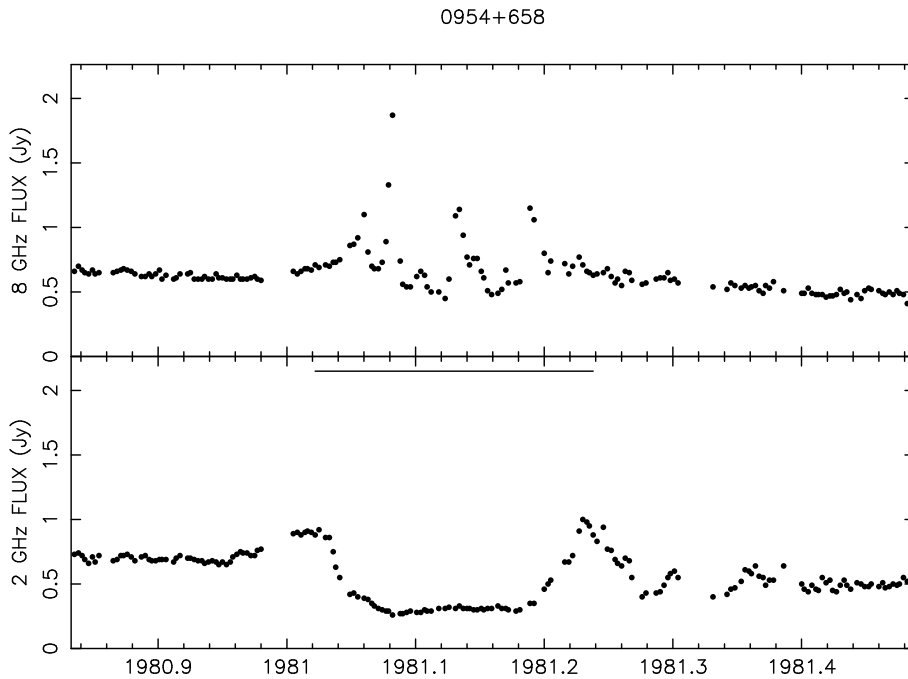


**Figure 8**

The first discovered ESE. Flux density at 8 GHz (top) and 2.7 GHz (bottom) of QSO 0954+658 obtained with the Green Bank Interferometer. The x-axis shows time in years. The dramatic decrease of the flux density at 2.7 GHz around 1981.2 yrs, accompanied with several sharp spikes at 8 GHz, is caused by refractive effects due to QSO's light encountering a dense plasma lens. From Fiedler et al. 1987.

light curve shapes has been discovered. Fiedler et al. (1994) also plotted positions of their 365 observed sources, as well as nine sources exhibiting one or more ESEs, and positions of four major Galactic radio continuum loops. The ESE events appeared to be in a statistically significant association with Loops I, II and III.

While Fiedler et al. (1994) provided a statistical model for flux redistribution based on stochastic broadening regardless of its nature (refractive or diffractive), Clegg, Fey & Lazio (1998) provided a detailed quantitative description of the optical properties of an interstellar plasma lens assuming that this is a discrete object (Figure 9). This model is still being used to estimate lens physical properties from observed light curves. The 1-D refractive properties

of the lens are specified by a dimensionless parameter  $\alpha$ :

$$\alpha = 3.6 \left( \frac{\lambda}{1 \text{ cm}} \right)^2 \left( \frac{N_0}{1 \text{ cm}^{-2} \text{ pc}} \right) \left( \frac{D}{1 \text{ kpc}} \right) \left( \frac{a}{1 \text{ AU}} \right)^{-2} \quad (10)$$

where  $\lambda$ ,  $N_0$ ,  $D$  and  $a$  are the wavelength of observation, maximum free-electron column density, distance from lens to observer, and size of the lens transverse to the line of sight, respectively. In the central portions of the lens, the overdensity of the plasma causes rays to spread (diverging lens) corresponding in the light curve to reduce intensity. Rays passing through the wings of the lens, where the density gradient is largest, are differentially refracted, leading to formation of converged rays, or caustics, which correspond in the light curve to spikes. The formation of caustics may be sensitive to the density profile, e.g a power law would behave differently from a Gaussian. If the lens were aspherical, the light curve would be sensitive to viewing angle. While these refinements are possible topics for the future, the Clegg et al. model has been remarkably successful in demonstrating the physical effects in play and reproducing many of the observed features of ESEs.

A second parameter,  $\beta_s$ , characterizes the extent to which the effect of the lens is diminished by the intrinsic size of the source:

$$\beta_s = \theta_s / \theta_l \quad (11)$$

where  $\theta_s$  and  $\theta_l$  are the angular sizes of the background source and the lens, respectively. For  $1/\beta_s \gg 1$  (lens much larger than the source) or  $1/\beta_s \ll 1$  (lens much smaller than the source), the expected amplitude variations are very small and are limited by the sensitivity of observations. For  $\beta_s$  of order unity, the behavior is more interesting, with deep flat minima and shallow rounded minima both possible. Yet, sources may have multiple components and complex morphology, the effects of which are not easily encapsulated by a single parameter, as perusal of Clegg et al.'s paper reveals.

By applying the model to light curves of two ESEs Clegg et al. estimated lens sizes of 0.065 and 0.38 AU and electron densities of  $n_e = 300$  and  $10^5 \text{ cm}^{-3}$ , respectively. The implied thermal pressures of  $P/k \sim 10^{6-9} \text{ K cm}^{-3}$  are very high and Clegg et al. concluded that such discrete, highly over-pressured lenses are either highly transient or are embedded in high-pressure environments. Both ESEs (0954+658 and 1741-038) were found to have likely associations with radio Loops III and I.

Besides explaining the minimum in the background source's light curve due to the presence of a diverging plasma lens, this model also predicted several additional observational effects: (1) the formation of caustic surfaces which have been observed in many ESEs (e.g. 0954+658 in Figure 8 shows caustic spikes at the start and end of the ESE event), (2) possible creation of multiple source images (discovered later in the case of 2023+335, Pushkarev et al. 2013), (3) angular position wander of the background source. While all these effects have been observed in ESEs supporting the discrete-lens model, some discrepancies between the model and observed light curves have been noticed since early days. Clegg et al. (1998) suggested that the discrepancies could be due to some combination of sub-structure within the lens, an anisotropic lens shape, a lens that only grazes the source instead of passing completely over it, or possibly unresolved sub-structure within the extragalactic source.

**3.1.2. More Recent Results.** Lazio et al. (2000) obtained VLBI imaging of PKS 1741-038 at four epochs during and after an ESE event. While multiple source images and the angular position wander were not detected, the source exhibited excess angular broadening during the ESE phase. However, the amount of angular broadening was larger than what is expected by simple refractive defocussing (Clegg et al. 1998). In addition, these four-epoch measurements hinted at the existence of an anti-correlation between the source flux density and angular diameter. Lazio et al. suggested a likely combination of refractive defocussing by a discrete lens and stochastic broadening caused by interstellar turbulence. This experiment shows a power of frequent monitoring of ESE sources. The correlations between the source flux density and angular broadening clearly needs further observations and testing.

As pointed by Fiedler et al. (1994) and many others, one of the key open questions about ESEs is their relationship with other phases of the ISM, specifically TSAS. Lazio et al. (2001a) is the only study of HI absorption of a source (PSR 1741-038) while it was undergoing an ESE. No changes in the HI absorption spectra, or rotation measure, were detected. Their upper limit on the HI optical depth was  $\Delta\tau < 0.05$ , marginally ruling out the existence of TSAS associated with this ESE. As this is the only such experiment, additional and even more sensitive measurements are needed to investigate possible connection between TSAS and ESEs.

Pushkarev et al. (2013) detected for the first time significant structural changes in QSO 2023+335 images over time, as well as changes in the light curve typical of an ESE at 15 GHz. The observations were obtained over 16 epochs (over 11 years) and similar structural changes were not found in  $\sim 300$  other AGN jet sources observed by the

Monitoring Of Jets in Active galactic nuclei with VLBA Experiments (MOJAVE) program. The observed structural changes are due to multiple imaging of the source induced by refraction in the intervening ISM. The angular separation between image peaks follows a  $\lambda^2$  dependence, in agreement with a plasma scattering origin of the induced sub-images. There are several additional unusual aspects of this source. First, while most ESEs are detected at 2 GHz, this is the only one detected at 15 GHz (as well as 8 GHz). Second, multiple ESE events have been noticed in the light curve of this source.

By fitting the light curve with the stochastic model by Fiedler et al. (1994), Pushkarev et al. estimated the apparent angular size of the lens ( $\theta_l = 0.27$  mas). As QSO 2023+335 is located behind the Cygnus supernova remnant, it was assumed that the lens is associated with the Cygnus region and is at a distance  $D = 1.5$  kpc. The transverse linear size of the lens is:  $a = \theta_l D = 0.4$  AU. The proper motion of the lens of  $6.8$  mas  $\text{yr}^{-1}$  results in the transverse lens speed of  $48.7$  km/sec. Using these estimates and equation (1), they obtained  $N_0 = 2.5 \times 10^{17}$   $\text{cm}^{-2}$  and a free-electron density within the lens  $n_e = N_0/a = 4 \times 10^4$   $\text{cm}^{-3}$ . Interestingly, their analysis of the angular broadening suggested an unusually steep turbulent spectrum with a slope 4.2-4.7. This suggests that the over-dense and over-pressured lens responsible for the observed ESE lives inside a scattering medium with an unusually steep turbulent spectrum. While the origin of such turbulence is still not clear, more shallow spectra were seen in previous studies and were associated with localized (instead of uniform) scattering screens.

Bannister et al. (2016b) argued that real-time detection is the key to understanding ESEs as most properties of the lens are measurable only while ESE is in progress (e.g.  $n_e$  profile, angular geometry of the lens, dust/neutral/magnetic field properties of the lens). A dedicated new, real-time search for ESEs is underway with the Australia Telescope Compact Array. About 1000 AGNs are being monitored once a month, with only 50 sec of integration time on target over the 4-8 GHz frequency range. An automatic search for changes in the continuum spectrum from a smooth distribution are used to identify new ESEs. Dedicated high-cadence monitoring is then performed for identified events. An exciting result from this campaign is the discovery of an ESE in the direction of PKS 1939-315 in 2014. The detailed monitoring allowed this study to model the  $N_e$  profile as a function of time. They found that the peak in the profile corresponds to the minimum of the flux density profile, suggesting a diverging lens. The column density changes of  $N_e \sim 10^{16}$   $\text{cm}^{-2}$  over transverse scales of  $\sim 10^{13}$  cm (corresponding to 20 days at an assume transverse velocity of 50 km/s), implied  $n_e \sim 10^3$   $\text{cm}^{-3}$  and  $P/k \sim 10^6$  K  $\text{cm}^{-3}$  (if no elongation along LOS assumed). The goal of this program is to generate a statistically significant sample in the future to determine covering fraction and spatial distribution of ESE lenses.

**Table 3** Summary of ESE events.

Source	Coords ( $^{\circ}$ )	Size (AU)	$n_e$ ( $\text{cm}^{-3}$ )	$N$ ( $\text{cm}^{-2}$ )	Reference
0954+658	146,43	0.4	$10^5$	$6 \times 10^{17}$	Clegg et al. 1998
1741-038	21.6,13.1	0.065	300.	$3 \times 10^{14}$	Clegg et al. 1998
0133+476	-	-	-	-	Fiedler et al. 1994
0300+470	-	-	-	-	Fiedler et al. 1994
0333+321	159.0,-18.8	-	-	-	Fiedler et al. 1994
1502+106	11.4,54.6	-	-	-	Fiedler et al. 1994
1611+343	-	-	-	-	Fiedler et al. 1994
1749+096	21.6,13.1	-	-	-	Fiedler et al. 1994
1821+107	-	-	-	-	Fiedler et al. 1994
2352+495	-	-	-	-	Fiedler et al. 1994
2023+335	-	0.4	$4 \times 10^4$	$2.4 \times 10^{17}$	Pushkarev et al. 2013
PKS1939-315	8.5,-24.0	0.7	$10^3$	$10^{16}$	Bannister et al. 2017
PSR J1643-1224	5.7,21.2	56.	130.	$10^{17}$	Maitia et al. 03
PSR B1937+21	57.5,-0.3	0.094	25.	$3 \times 10^{13}$	Cognard et al. 93
PSR B1937+21	57.5,-0.3	0.05	220.	$2 \times 10^{14}$	Cognard et al. 93
PSR B1937+21	57.5,-0.3	0.6	200.	$2 \times 10^{15}$	Lestrade et al. 98
PSR B1800-21	8.4,0.1	220.	15000.	$5 \times 10^{19}$	Basu et al. 2016
PSR J1603-7202	316.6,-14.5	4.9	3.4	$2 \times 10^{14}$	Coles et al. 15
PSR J1017-7156	291,-12.6	13.9	3.7	$8 \times 10^{14}$	Coles et al. 15
0133+476	131,-14	-	-	-	Lazio et al. 2001
0201+113	150,-47	-	-	-	Lazio et al. 2001
0202+319	141,-28	-	-	-	Lazio et al. 2001
0300+470	145,-10	-	-	-	Lazio et al. 2001
0528+134	191,-11	-	-	-	Lazio et al. 2001
0952+179	216,48	-	-	-	Lazio et al. 2001
0954+658	146,43	-	-	-	Lazio et al. 2001
1438+385	66,65	-	-	-	Lazio et al. 2001
1502+106	11,55	-	-	-	Lazio et al. 2001
1756+237	49,22	-	-	-	Lazio et al. 2001
2251+244	92,-31	-	-	-	Lazio et al. 2001
2352+495	114,-12	-	-	-	Lazio et al. 2001

Note that nine ESEs were discovered by Fiedler et al. (1994) but do not have estimated size and density of the intervening lenses. ESEs detected in Lazio et al. (2001) by applying a wavelet analysis on the Green Bank Interferometer monitoring data also do not have estimated size or density.

**Figure 9**

A schematic diagram of refraction by a Gaussian plasma lens from Clegg et al. 1998. The top panel shows ray paths. Rays which pass near the cloud center diverge, while ray paths which pass through the sloping edges are differentially refected and converge, forming caustics.

**3.1.3. Pulsar ESEs.** Similar dramatic changes in the flux density have been seen in the case of several pulsars. Cognard et al. (1993) observed a sudden decrease in the flux density of PSR1937+21 over a period of 15 days, coupled with an increase in the time of arrival of the pulses from this millisecond pulsar. These observations are modeled as resulting from perturbations in the dispersive delay (caused by DM fluctuations which are proportional to fluctuations in the electron density), and the geometric refractive delay (caused by the intervening ionized screen and being proportional to the refraction angle and the distance to the screen). The best fit was obtained for a two-component model with electron densities of 25 and 220 cm<sup>-3</sup>, respectively, and corresponding transverse structure lengths of 0.094 and 0.05 AUs. While the inferred densities are lower than what is typically found for ESEs, they still imply a large over-pressure problem. PSR1937+21 is in close angular proximity to the Cygnus loop and Cognard et al. concluded that these observations support models for ESE production near peripheries of expanding superbubbles. Finally, they suggested that pulsar ESEs could be the dominant source of timing noise in pulsar observations and need to be considered when searching for signatures of gravitational waves in pulsar timing measurements. Lestrade, Rickett & Cognard (1998) analyzed observations of the same pulsar over an even longer period and identified several additional ESEs. For the Oct 1989 event (same as in Cognard et al. 1993) they estimated approximate transverse size of 0.6 AU assuming the velocity of 50 km/s, and density of 200 cm<sup>-3</sup>. Their work showed how difficult it is to identify ESEs.

Basu et al. (2016) studied PSR B1800-21 at several frequencies using the GMRT. This is a young pulsar within the W30 complex which contains a SNR and a number of HII regions. This pulsar, and a handful of others, exhibited a significant evolution during the observing period with the low-frequency part of the spectrum becoming steeper for a period of several years before reverting back to its initial shape. The most likely reason for the turnover is free-free absorption by the intervening medium, whose properties have been estimated as having a size of 220 AU and  $n_e \sim 1.5 \times 10^4$  cm<sup>-3</sup>. While this was not a classical pulsar ESE event, the observed properties are very much in the ESE range.

Coles et al. (2015) showed two pulsar ESE events with the corresponding dispersion observations. The ESEs were seen at the same time in DM fluctuations ( $\delta DM$ ), the coherence bandwidth ( $\nu_0$ ) and the intensity timescale ( $\tau_0$ ), and were identified by eye. The estimate size is about 5-14 AU and  $n_e \sim 4$  cm<sup>-3</sup>. The DM fluctuations were 0.0023 and 0.0015 pc cm<sup>-3</sup>, respectively. However, in addition they found several cases of significant DM fluctuations that did not have the corresponding changes in the coherence bandwidth or time fluctuations and therefore would not be identified as ESE. We summarize basic observed properties of ESEs in Table 3.

## 3.2. Theory of Ionized Structures

**3.2.1. Refraction Basics.** The theory of scintillation - both wave propagation and how it translates to observables - is well documented elsewhere (Rickett 1977, 1990), so we only quote a few basic results here. The refractive index  $n_r$  of electromagnetic waves in a plasma is:

$$n_r = \left(1 - \frac{\nu_{pe}^2}{\nu^2}\right)^{1/2} \sim 1 - \frac{\nu_{pe}^2}{2\nu^2}, \quad (12)$$

where  $\nu_{pe} \equiv (n_e e^2 / \pi m_e)^{1/2} = 9.0 \times 10^3 n_e^{1/2} \text{s}^{-1}$  is the electron plasma frequency and the second relation holds for  $\nu_{pe}/\nu \ll 1$ , which generally holds for observations of the ISM.

According to eqn. (12), radio frequency waves have group velocity  $v_g \sim c(1 - \nu_{pe}^2/2\nu^2)$ . Pulsar pulse arrival times  $t_p$  therefore depend on  $\nu$ ;  $dt_p/d\nu \propto \nu^{-3}$ . This can be used to derive the total electron column density, or dispersion measure DM, between the pulsar and Earth. The importance of this goes beyond its value as a probe of the ISM. Pulsar pulse arrival times are sensitive to low frequency gravitational waves in the spacetime between the pulsar and the Earth (van Haasteren 2014). The dispersion in pulse arrival times caused by the theoretically predicted gravitational wave background is typically tens to hundreds of nanoseconds, while temporal variations in DM cause dispersion of a few  $\mu\text{sec}$ . This creates a huge incentive to monitor and model temporal variations of DM and all other plasma effects so they can be properly accounted for in analyses of pulsar timing. Serendipitously, pulsar timing data can be used to monitor electron density structure in the ISM (Lam et al. 2016).

Variation of  $n_e$  with position on scales large compared to a wavelength causes refraction. Equation (12) can be

used to explain the divergence of rays shown in Figure 9. The waves are refracted toward regions of lower phase speed, which are regions of lower electron density (see eqn. (10)). Variations of  $n_e$  also cause variation of the source intensity, angular broadening and, in the case of pulsars, temporal broadening. It can be shown from the equations of geometrical optics that a wave of wavelength  $\lambda$  which propagates a distance  $L$  through density fluctuations with transverse scale  $l_\perp$  and amplitude  $\Delta n$  is scattered through an angle  $\Delta\theta_0$  of order  $r_e\lambda^2(L/l_\perp)\Delta n$ , where  $r_e \equiv e^2/m_e c^2$  is the classical electron radius. Over the distance  $D$  to the source the time of flight of a ray deflected into our line of sight is increased by  $\Delta\tau \sim D(\Delta\theta_0)^2/c$ . If there are  $N \propto D$  deflections and the  $\Delta\theta$  have a Gaussian distribution with rms value  $\Delta\theta_0$ , then the temporal broadening of pulses should scale with distance, density fluctuation amplitude, and wavelengths as  $D^2(\Delta n)^2\lambda^4$ .

**3.2.2. Nature of the fluctuations.** Soon after the discovery of pulsar scintillation (Rickett 1970), it was pointed out by Scheuer & Tsytovich (1970) that the models in which the density fluctuations are plasma waves require special conditions and large energy inputs. Scheuer & Tsytovich (1970) estimated the power requirements to be about  $1.6 \times 10^{-24} \text{ erg cm}^3 \text{ s}^{-1}$ , which is almost an order of magnitude larger than the energy input from supernova explosions and 2-3 orders of magnitude higher than the power supernovae supply to the kinetic energy of the ISM. Although one may quibble with the characterizations of the fluctuation spectrum and its dissipation mechanisms in Scheuer & Tsytovich (1970), their basic points that ion-neutral damping is strong in partially ionized regions, and that wave dissipation is strong at these short wavelengths, remain valid and impose strong constraints on any theory for interstellar scintillation.

Motivated in part by the high density and ionization fractions inferred for the scattering environment, attention turned to ionized portions of the ISM as the source of scintillation. The collisionally ionized gas in the ISM (HIM) is probably too low in density to be the site of TSIS, but warm, photoionized gas (the WIM) has a moderately large filling factor and typically density  $n_H \sim 0.05 - 0.1 \text{ cm}^{-3}$ . We distinguish the WIM from H II regions around hot stars, which can be quite dense and overpressured, and from the edges of clouds, which can also be overpressured if the clouds are self gravitating. After ionized gas was identified as the source of scintillation, the question of whether the host medium was confined or pervasive remained. However, large density enhancements, and therefore large densities, were favored.

Higdon (Higdon 1984, 1986) proposed an ingenious solution to the energetics problem. In his picture, the density fluctuations arise from essentially static entropy modes, which are nearly isobaric ( $\delta n/n \sim -\delta T/T$ ) and cascaded from large to small scales due to interacting with a turbulent, highly anisotropic spectrum of MHD waves propagating almost perpendicular to the background magnetic field. In this scenario,  $n_e$  is merely a passive scalar. Higdon argued that such waves are relatively weakly damped, and that because they are driven by a cascade originating at large scales, they tap into the global energy reservoirs in the ISM. Although Higdon considered a number of physical settings, he ultimately favored turbulence driven by evaporating clouds in HII regions surrounding hot stars, which drive both thermal and dynamical perturbations to the surrounding medium, as the sites where scintillation is produced (Higdon 1986).

Higdon's ideas were extended and made more rigorous in a series of papers on interstellar turbulence beginning with Goldreich & Sridhar (1995) and culminating with Lithwick & Goldreich (2001). These papers developed the theory of anisotropic, turbulent cascades of shear, compressionless Alfvén waves. The anisotropy scaling within the inertial range of the Goldreich-Sridhar spectrum can be derived by assuming constant energy flux in  $k$  space ( $k_\perp v_\perp^3(k_\perp) \sim k_0 v_A^3$ ) and that the turbulence is critically balanced ( $k_\perp v_\perp(k_\perp) \sim k_\parallel(k_\perp) v_A$ ), where  $k_0$  is the scale at which the turbulence becomes Alfvénic. As we noted in §1.3, these two relations lead to elongated contours of constant power in  $k$ -space with  $k_\parallel/k_\perp \sim (k_d/k_\perp)^{1/3}$ . Strictly this only means that contours of constant power in the  $(k_\perp, k_\parallel)$  plane are elongated, but coherent structures tend to be aligned with the magnetic field as well.

When weak compressibility effects are included, the turbulence can be resolved into three wave modes: the shear Alfvén mode, which is compression free, and the fast and slow magnetosonic modes. While both magnetosonic modes produce density fluctuations, the slow mode is more compressive and has a spectrum similar to the Kolmogorov spectrum (Cho, Lazarian & Vishniac 2002), in agreement with the scintillation measurements. Thus, there are two sources of density fluctuation in the Lithwick & Goldreich (2001) theory: entropy modes and slow modes.

The slow modes may be important. As Lithwick and Goldreich pointed out, when the cooling time of the entropy modes is short compared to the eddy turnover time at their scale, they are heavily damped, and therefore cannot be cascaded from large scales. And, the power spectra of passive scalars are in general not the same as that of the turbulent velocity fluctuations that mix them (Shraiman & Siggia 2000; Warhaft 2000), but have exponential tails and a highly intermittent spatial distribution. As of this writing, the electron density fluctuation spectrum produced



by entropy and MHD modes under ISM conditions, i.e. with realistic damping, cooling, and recombination has not yet been definitely calculated. While the observed spectrum of density fluctuations is roughly in agreement with expectations for slow magnetosonic turbulent modes, it is still not understood why and how the observed spectrum persists to very small spatial scales where theoretically we would expect the entropy modes to be heavily damped.

**3.2.3. Distribution of scattering material.** The dependence of scattering on source distance and location in the Galaxy provides important information that complements what can be gleaned from the power spectrum. We showed earlier in this section that if the angular deflection of radio waves due to scattering follows Gaussian statistics, then the widths of pulsar pulses should scale with wavelength and distance as  $\lambda^4 D^2$ . However, for pulsars with dispersion measures (or electron column densities) greater than about  $20 \text{ cm}^{-3} \text{ pc}$ , the relationship is better fit by  $\lambda^4 D^4$ . This was taken as evidence by Cordes, Weisberg & Boriakoff (1985) that the scintillation cannot be entirely due to a pervasive homogeneous medium but must include a contribution from localized clumps within which enhanced scattering occurs.

The two component model was formalized and generalized in a series of papers by Boldyrev and Gwinn. In Boldyrev & Gwinn (2003); Boldyrev & Königl (2006) it is argued that the  $D^4$  scaling of the pulse width with distance can be explained if the distribution of  $\Delta\theta$  is not Gaussian, but rather is described by a Levy distribution. Levy distributions have a divergent second moment. Thus, quantities such as the mean squared scattering angle  $(\Delta\theta)^2$  or pulse width  $\tau$  are dominated by a few of the largest scattering events. Whereas in a Gaussian model the mean squared angular deviation scales linearly with  $D$  and the time delay therefore scales as  $D^2$ , the observations suggest that the mean squared angular deviation scales as  $D^3$ . A  $\Delta\theta$  distribution  $P(\Delta\theta) \propto |\Delta\theta|^{-5/3}$  will lead to this dependence.

Remarkably, Boldyrev & Königl (2006) showed from geometric arguments that rays passing through thin shells of ionized gas are scattered according to just such a distribution. The “rare events” in this case correspond to ray paths that just graze the inner edges of the shells, resembling sheets seen edge on. They suggested that the scattering arises in the ionized edges of molecular clouds near luminous hot stars and present quantitative arguments for the properties of these shells:  $n_e \approx 10^2 \text{ cm}^{-3}$ , shell thickness of  $\sim 0.003 \text{ pc}$ , cloud radii of about  $10 \text{ pc}$ , and cloud separations of about  $100 \text{ pc}$ . The ionized shells may themselves become turbulent, leading to additional scattering.

**3.2.4. Kinetic effects.** An entirely different physical explanation for a similar Levy distribution was proposed by Terry & Smith (2007, 2008); Smith & Terry (2011). These authors studied decaying Alfvén turbulence down to wavelengths of a few to tens of thermal ion gyroradii  $r_i \equiv (k_B T_e / m_i)^{1/2} / \omega_{ci}$ . In contrast to the shear Alfvén waves in the magnetohydrodynamic cascade, which do not have density fluctuations, as the wavelength approaches  $r_i$  the electron density begins to fluctuate in tandem with fluctuations in the parallel current such that:

$$\frac{\delta n_e}{n_e} \sim \frac{\delta B_\perp}{B} \frac{k_\perp r_i}{(1 + k_\perp^2 r_i^2)^{1/2}}. \quad (13)$$

Thus, while at long wavelengths electron density is advected like a passive scalar, at the short lengthscales associated with pulsar scintillation, density fluctuations play a key role in the dynamics of the waves, which in this regime are known as kinetic Alfvén waves. When nonlinear effects are included, electrons form coherent sheets and filaments with density profiles that scatter radio waves according to the same  $\Delta\theta$  distribution as thin shells. To the extent that the shells are turbulent, with turbulence extending to kinetic scales, the two pictures are not mutually exclusive.

The question of what is the *minimum* scale for kinetic Alfvén wave turbulence is not fully resolved. At  $k_\perp r_i \geq 10$ , the waves are collisionlessly damped by electrons, but Howes, Tenbarge & Dorland (2011) found that turbulent power persisted down to the electron gyroscale  $r_e$ , consistent with the range of scales observed in the solar wind. Evidence that the electron density fluctuations extend to scale as small as  $70 \text{ km}$ , as small as  $r_r$ , is presented in Rickett et al. (2009) and reviewed in Haverkorn & Spangler (2013).

At this point, there is no clear consensus on the nature of the electron density fluctuations revealed by pulsar scintillation. It is probably safe to say that they occur in gas that is nearly fully ionized and denser than the hot, collisionally ionized component or warm diffuse component that is not specifically associated with bright stars. Whether they are produced by an underlying turbulent process or are associated with particular types of object is less clear. When we consider that the pulse width-distance relation can in principle, be produced by scattering from thin shells of ionized gas  $10 \text{ pc}$  in size, or electron filaments and sheets  $1000 \text{ meters}$  in size, and that H II regions, cloud edges, and supernova shells can all host turbulence with Kolmogorov features, the possibilities seem wide indeed.

**3.2.5. ESEs.** An important related question is whether ESEs are a more extreme but qualitatively similar form of scattering (Hamidouche & Lestrade 2007) or are a signature of something entirely different. The ESE discovery paper Fiedler et al. (1987b) suggested that the transient brightness dip is due to refraction by an overdense “plasma lens”

with projected size on the sky of a few AU. We reviewed the properties of plasma lenses in §3.1, and only note here that the recent work of Bannister et al. (2016b) is considered to rule out underdense, magnetically structured lenses such as suggested by Pen & King (2012). If such lenses are roughly spherical then  $n_e \sim 10^3 - 10^4 \text{ cm}^{-3}$ , which together with typical ionized gas temperatures  $T \sim 10^4 \text{ K}$  imply pressures at least  $10^3$  times higher than the typical ISM pressure. It was immediately appreciated that without a confinement mechanism such structures could survive for at most a few years.

If the lenses are thin, turbulent sheets viewed end on they could have high column density without high volume density, thus reducing the overpressure problem. For example, if the elongated structures followed Goldreich-Sridhar scaling, the mean density of a structure viewed end on would be  $(l_{\perp}/l_{\parallel})^{2/9}$  smaller than if the structure were spherical; for  $l_{\perp} = 10^{13} \text{ cm}$ ,  $l_{\parallel} \sim 1 \text{ pc}$ , this is a factor of .06. However, because of the small transverse dimension, extremely thin substructure is still required. In the model of Romani, Blandford & Cordes (1987), the extreme brightening arcs are due to caustics, or converging ray paths; in the turbulent walls of old supernova remnants seen edge on.

Walker & Wardle (1998) and Wardle & Walker (1999) attempted to solve the high pressure problem for ESEs by suggesting that the refraction occurs in ionized evaporative outflows from cold, self gravitating clouds a few AU in size. If the clouds have velocity dispersions characteristic of halo objects, their motion through all but the hottest portions of the ISM drives bowshocks, and creates a hot gas layer between the shock and the cloud which intensifies the evaporation, and possibly draws out a turbulent magnetotail. All of these phenomena create dense, small scale structure which may explain a variety of ESE light curves and pulsar scattering properties. Based on a covering factor  $f_c \sim .005$  (Fiedler et al. 1994), the tiny clouds postulated by Walker & Wardle are a major form of dark matter in the Milky Way (optical lensing by similar clouds was proposed by Draine (1998) as the source of microlensing in dark matter surveys). However, as noted in § 3.3 statistics are still poor, so it is possible that  $f_c$  is lower and the clouds are more rare. The ongoing monitoring project for ESEs will place valuable constraints on  $f_c$ . More fundamentally, McKee (2001) showed that self gravitating, polytropic clouds with the low surface pressures and high total column densities proposed for the ESE models cannot be heated sufficiently by standard mechanisms to offset radiative cooling. While it may be possible to create composite models with a polytropic index that varies from core to envelope by fine tuning, but this throws up a serious roadblock to self gravitating clouds as a source for ESEs.

In our view, a turbulent origin of ESEs cannot be ruled out, but it probably requires a special environment in which driving is so strong that the cascade reaches kinetic scales at which electrons and ions decouple. Although ray tracing has been carried out for the plasma lenses reviewed in §3.1.1, we are not aware of any comparable study for electron turbulence. Since simulations of such turbulence are now available, this is a viable project for the future.

### 3.3. Summary and Outstanding Questions

**Abundance.** In total, no more than 35 ESEs have been discovered so far (Pushkarev et al. 2013). We list in Table 3 their observed properties from the literature. The first one is the ESE from the discovery paper by Fiedler et al. (1987) that was studied by several authors. Fiedler et al. (1994) discovered 9 additional ESEs, however they did not derive lens size and electron density. We list these sources in the table for completeness and potential future followups. With over 300 sources observed and only 10 ESEs detected in over 11 years, Fiedler et al. (1994) estimated the rate of ESE occurrence as  $\sim 0.017$  events per source-year. Lazio et al. (2001b) performed probably the most systematic search so far. They monitored 149 sources with the Green Bank Interferometer every 2 days spanning 17 years and applied a wavelet-based technique to identify ESEs from the source light curves. They discovered 15 ESE (lens size and density were not provided), however their wavelet technique failed to pick up several previously identified ESEs. In Pushkarev et al.'s MOJAVE sample of  $\sim 300$  AGNs only one ESE was found. The current monitoring program by Bannister et al. is targeting 1000 AGNs and at least three ESEs have been discovered so far Bannister et al. (2016b,a).

While the statistical samples are small and the frequency of ESE events is still not properly established, it is clear that these are rare events. Many authors have pointed out, however, that identification of ESEs is very difficult. For example, short-timescale and small-amplitude ESE can be confused with interstellar scintillation, while long-timescale and small-amplitude ESE can be obscured by an intrinsic source variability. The exact definitions of how to identify and classify small- from high-amplitude variability is tricky. At the same time, the connection between discrete lenses (commonly used in ESE interpretation) and the turbulent ionized medium the signal from background sources is traveling through is still not clear. One reasonable assumption could be that event timescales and amplitudes fall in a continuous range that merge both scintillation and intrinsic variability. In addition, most ESEs have been discovered serendipitously. As ESE events can start at any time, it is unclear whether the cadence of observational experiments has been good enough in previous experiments. Frequent and dedicated monitoring, like in Bannister et al., is needed to provide proper statistical samples and estimates of the volume filling factor of ESEs.

ESE identification methods so far have been rather simplistic. Most studies have identified ESE from light curves by eye. With larger monitoring programs systematic and automatic ESE searches are essential. Lazio, Waltman, Ghigo et al. (2001) tested several statistical tools, in particular the wavelet transform of the light curves. It is encouraging that they found 15 events in the light curves of 12 sources, however five ESEs previously identified by hand did not pass their wavelet selection criteria. This clearly requires further attention. Bannister et al. are taking a new approach by monitoring AGN continuum spectra once per month over the 4-8 GHz frequency range, searching for sudden changes in the flux density *vs* frequency spectra. As the plasma refractive index depends on  $\lambda^2$ , large departures from the power-law flux density spectra are expected at the start of an ESE event. In addition, as suggested by Clegg et al. (1998), followup imaging observations right from the start of an ESE can provide information about angular displacements and multiple images which can assist in the interpretation of light curves. This requires very high resolution monitoring (e.g. with VLBI) as changes can occur on milli-arcsecond, or even smaller, angular scales.

**Likely sites of ESEs.** Since early days a possible connection between SNRs and ESEs has been proposed. Fiedler et al. (1994) noticed angular proximity of nine ESEs with Loops I, II and III. ESE in the direction of QSO 2023+335 is positioned behind the Cygnus SNR. The ESE in the direction of PSR B1937+21 is also likely associated with a SNR shell. We view detailed modeling of turbulence in and surrounding supernova remnants as a promising line of future research. Beyond the works of Romani, Blandford & Cordes (1987); Boldyrev & Königl (2006); Lam et al. (2016), our understanding of turbulence associated with supernova driven shocks is growing rapidly due to its serendipitous connection with cosmic ray acceleration and transport (Amato 2014). This includes study of the interaction between the shock and pre-existing density irregularities, which generates turbulence both downstream (Beresnyak, Jones & Lazarian 2009) and upstream (Drury & Downes 2012) of the shock. While these and other modelers have not had ESEs or other electron density fluctuations in mind, their work could be a springboard for a new study of small scale structure associated with supernova remnants.

**Internal structure.** Many studies have pointed out that understanding of the internal, and possibly multi-phase nature, of ESE lenses is still unconstrained. Only one ESE was followed up with a HI absorption experiment. While this experiment marginally excluded the possibility of TSAS existing along the same line of sight during the duration of the ESE, more sensitive observations are clearly needed. Additional measurements are necessary to investigate a possible TSAS-ESE connection. Draine (1998) suggested that if ESE lenses have a molecular component there should be detectable H<sub>2</sub> vibrational absorption lines. James Webb Space Telescope (JWST) would provide an excellent possibility to search for H<sub>2</sub> associated with ESEs. Detecting these transitions during a lensing event would confirm the gaseous nature and determine the lens radial velocity, providing an “unambiguous signature of gaseous lensing”. In addition, for IDV and intra-hour variable sources with nearby scattering screens, a deep search for the associated molecular gas with ALMA, as well as deep H $\alpha$  imaging to search for the ionized component, may be possible (Hayley Bignall, private communication).

Furthermore, detecting DM variations due to an ionized TSAS skin are now possible due to extremely high-precision pulsar timing for gravitational wave detection. Lam et al. (2016) estimated that the DM increase due to a pulsar passing behind an ionized structure of electron density  $n_e$  is:  $10^{-5} n_e l_{10 AU} \text{ pc cm}^{-3}$ , where  $l_{10 AU}$  is the pathlength through the structure. For a TSAS of 100 AU in size and density of  $10^3 \text{ cm}^{-3}$ , this would suggest  $10^{-5} \times 10^3 \times 10 \times 10^{-2} = 10^{-3} \text{ pc cm}^{-3}$ , assuming that only 1% of the TSAS diameter is in the ionized skin. Similarly, as pulsars move through the neutral medium they can ionize their surroundings and form bow shocks essentially making their own scattering medium (as distinct from their magnetospheres). Considering typical pulsar parameters, Lam et al. (2016) estimated the bow shock scales of AU to 0.1 pc and the resultant increase in DM increase at a level of  $3.3 \times 10^{-3} \text{ pc cm}^{-3}$ . This is typically of order  $10^{-3}$  of the mean DM.

**The formation mechanism: discrete lenses or fluctuations in the turbulent cascade?** As we have shown so far, many parallel questions concerning the origin of TSAS and ESE still remain. The issue of whether ESE properties can be explained as being due to the turbulent cascade in the ionized medium, as opposed to discrete blobs or lens, is one of those questions. Detection of multiple images in particular lends support to the discrete lens model, yet only one or two such cases have been observed. On the other hand, properties of most pulsar ESEs appear to be more mild, in terms of size and density, than those of ESEs discovered in the direction of extragalactic sources. This could be real, or due to some non-understood systematic differences in observing methods. In fact, Hamidouche & Lestrade (2007) argued using simple simulations that pulsar ESEs can be explained with Kolmogorov turbulence.

The famous big power-law by Armstrong et al. (1995) was compiled from pulsar and extragalactic observations. For the finite-size extragalactic observations, Armstrong et al. (1995) used the observed refractive index  $n_r$  and source angular size (with an assumed distance to the scintillating medium of 500 pc) to estimate the amplitude of the power spectrum of electron density fluctuations,  $C_n^2$ , by using equation (17) from Coles et al. (1987). The power spectrum

of electron density fluctuations is defined as:

$$P_{\delta n_e}(q) = C_n^2 q^{-\alpha}, \quad (14)$$

where  $q = 1/l$ , with  $l$  being the size or spatial scale of fluctuations. Under the assumption that all sources trace the same ionized medium, a Kolmogorov slope of 11/3 was used to estimate  $P_{\delta n_e}(q)$  from the above equation. As a single power-law function can be fitted through all measurements of  $P_{\delta n_e}(q)$ , this is interpreted as electron density fluctuations in the ISM following a universal turbulent cascade.

As an illustrative example only we asked the question of where would ESEs toward extragalactic sources land in this Big Power Law graph. The Pushkarev et al. ESE in the direction of QSO 2023+335 is a clear example of strong scattering (due to the presence of caustics and multiple images), so we can assume that in this case  $n_r \sim 1$ . Following the same procedure then used in Armstrong et al. we estimate  $C_n^2 \sim 20 \text{ m}^{-6.67}$  and  $P_{\delta n_e} \sim 7 \times 10^{38} \text{ m}^{-3}$  at  $l = 6 \times 10^{10} \text{ m}$ . If we apply the same calculation on PKS 1939-315 (Bannister et al. 2016b), we get  $C_n^2 \sim 2 \times 10^{-2} \text{ m}^{-6.67}$ . The  $C_n^2$  values for both sources are higher (by a factor of  $\sim 10^4$  and  $\sim 10$ , respectively) relative to Armstrong et al.'s  $C_n^2 = 10^{-3} \text{ m}^{-6.67}$ . However, these values are not hugely off when considering the dispersion of the Big Power Law relation. While these are illustrative examples, they show that a turbulent origin of ESEs cannot be ruled out.

**Theory.** While overpressure is not a problem for “normal” pulsar scintillation, the evidence for structure on scales as small as 100 km provides a fascinating laboratory for magnetized plasma turbulence from fluid to kinetic scales. While the solar wind is also such a laboratory, and one that can be probed *in situ*, the wind is less collisional and known to be dominated by supersonic flow. At the smallest scales at which structure is observed, the electrons and ions are largely decoupled and we are in the regime of electron fluid turbulence (Biskamp et al. 1999; Cho & Lazarian 2009), which is known to develop intense filamentary structures. Whether such turbulence has properties compatible with TSIS, and what power source is necessary to sustain it, have yet to be determined. For more extreme structures, a theory for the formation of “plasma lenses” is sorely needed, both to complete the concept and to constrain the models (e.g. Gaussian vs power law slopes). The multiple sheets structures posited by Romani, Blandford & Cordes (1987) should also be amenable to numerical simulation.

#### 4. Future advances, observational and theoretical

The nature of turbulent dissipation processes, structures they produce and their local impact on dynamics and energy balance in the ISM remain at the frontier of astrophysics (Hennebelle & Falgarone 2012). TSAS and TSIS probe spatial scales in the ballpark of what is currently expected for dissipation scales, therefore offering a unique peek at important and not-well understood physical processes with huge implications for many areas of astrophysics. Similarly, as we demonstrated in this review, the heating rates due to expansion of over-pressured TSAS and ESEs could be significant, meriting measurements of the filling factor of these structures across different interstellar environments. In our view, TSAS and TSIS are not only important for understanding turbulent dissipation, but also offer a unique probe of the efficiency of stellar feedback as are likely produced by local turbulent enhancements in places like SNRs, stellar bubbles and winds. In light of the importance of stellar feedback and turbulence for many areas of astrophysics, we think that TSAS and TSIS deserve a major spotlight and attention. At the same time, demands for increasing precision in pulsar timing for low frequency gravitational wave detection is spurring efforts and building a new data base for modeling electron density fluctuation in the ISM. Many upcoming advances in both observational facilities and theory will enable progress in the field.

Several upcoming radio facilities are promising a revolution in terms of angular resolution and sensitivity: the Australia Square Kilometre Array Pathfinder (ASKAP), MeerKAT, Next Generation VLA (ngVLA), the Square Kilometre Array (SKA). This will provide excellent opportunities for interferometric imaging of HI absorption, at high resolution, toward extended radio sources, e.g. SNRs. The goal is to measure the power spectrum of  $\Delta\tau$  variations over a continuous range of scales from  $\sim 10 \text{ pc}$  all the way to  $\sim 10 \text{ AU}$  to test the turbulent origin of TSAS for a statistically significant and diverse sample of interstellar environments. Such experiments can probe the turbulent spectrum, but also improve understanding of the cut-off scales imposed by thermal conduction, ambipolar diffusion and other processes. As a complement, the Five-hundred-meter Aperture Spherical radio Telescope (FAST) will be a wonderful telescope for long-term monitoring of TSAS discovered via pulsar observations simultaneously at HI and OH frequencies. Long-term monitoring will build variations of  $\Delta\tau$  over spatial scales and reveal a roadmap of TSAS evolution with time. The ongoing revolution in the integral field spectrograph (IFU) astronomy will similarly provide optical absorption spectra simultaneously against hundreds of stars in clusters, enabling essentially 2D coverage and spatial power spectrum calculations using many species, which are currently not possible.

Another advantage some of these telescopes have is a large field of view (e.g. ASKAP, MeerKAT, SKA). Surveys

under planning (Dickey et al. 2013; McClure-Griffiths et al. 2015) will provide close to a million Galactic HI absorption spectra (SKA). This will provide rich constraints on the range of spin temperatures found and their spatial variations with interstellar environments, probing the dependence of heating and cooling, and thermal pressure, on the local environment. For understanding TSAS/ESE internal structure ALMA searches for CO, HCO<sup>+</sup>, CH<sup>+</sup> and SiO will be essential to understand cooling and a possible shock-related origin of these structures. Similarly, shock tracers can probe the immediate surrounds of TSAS; if TSAS is expanding into the CNM strong shocks are expected. Also, the James Webb Space Telescope (JWST) will be a wonderful instrument for measuring H<sub>2</sub> vibrational transitions in infrared, further constraining internal structure of both TSAS and ESEs.

Due to the “searchlight” nature of absorption profiles, exploring the temporal variability of absorption profiles will become abundantly more possible in the future. For example, ASKAP can stare at the Magellanic Clouds and in 50-200 hours of telescope time get an instantaneous sample of hundreds of HI absorption lines. A repeated experiment over several time epochs will provide hundreds of  $\Delta\tau$  probes. This is much cheaper in terms of telescope time than what is doable currently. Similarly, MeerKAT and SKA observations at different epochs will easily provide thousands of  $\Delta\tau$  measurements.

As we highlighted earlier, pulsars have a unique ability to probe neutral, ionized and molecular media over exactly the same line of sight. But dedicated experiments are required. One potentially interesting way to do this is by adding spectral-line observations to pulsar timing measurements for the sample of sources observed by the North American Nanohertz Observatory for Gravitational Waves (NANOGrav) collaboration. These pulsars are being monitored frequently to search for gravitational waves, however provide observations of DM over many time epochs that represent a goldmine for monitoring electron density structure in the ISM.

One of the key science goals of one of the several survey science projects accepted for ASKAP, VAST – Variables and Slow Transients - is to determine the origin and nature of structures responsible for ESEs. ASKAP will allow moderate sensitivity but wide field of view surveys (30 deg<sup>2</sup> in a single pointing) enabling fast surveys and searches for transient sources, Murphy et al. 2013. For example, Fiedler et al. (1994) searched about 600 sources in total for ESEs, VAST will be able to cover close to 180,000 source-years. This will help to constrain the frequency and spatial distribution of refractive lenses, and possible associations with Galactic structures. In addition, real-time follow-up monitoring will be provided of identified ESE sources – this is crucial for probing the possible connection with neutral structures, and to constrain magnetic field strength.

There are frontiers on the theory side as well. Advances in understanding magnetized turbulence down to kinetic scales can and should be applied to the ISM. As challenging as this is on its own, accounting properly for factors such as realistic heating and cooling processes, chemical reactions, suppression of thermal conduction and viscosity perpendicular to the ambient magnetic field, and the presence of cosmic rays are all essential for understanding the spectrum, degree of spatial intermittency, and nature of dissipation. In order to connect with observations, and make predictions, it will be necessary to consider radiation transport through the medium as well. Fortunately, with computational power increasing on rapidly, numerical simulations covering an extended range of scales that reaches down to AU scales are becoming more feasible, and it is allowing comprehensive modeling of bubble walls and supernova shells with unprecedented fidelity.

## DISCLOSURE STATEMENT

If the authors have nothing to disclose, the following statement will be used: The authors are not aware of any affiliations, memberships, funding, or financial holdings that might be perceived as affecting the objectivity of this review.

## ACKNOWLEDGMENTS

We are grateful for many inspiring discussions and thought provoking comments from the following colleagues, which have greatly improved the paper: Haley Bignall, Avinash Deshpande, Miller Goss, Carl Heiles, David Kaplan, Joe Lazio, Chris McKee, Dave Meyer, Steve Spangler, Jacco van Loon, Joel Weisberg, and Mark Wolfire. We also appreciate and thank the following undergraduate students at UW for their help with the manuscript. Delano Yoder assisted in collecting information for Tables 1 and 2. Sam Szotkowski compared heating and cooling rates from several publications, and Eowyn Liu assisted in the reference compilation. We thank Roselyn Lowe-Webb at Annual Reviews for her patience with the completion of this manuscript, as well as help with the last-minute LaTeX questions. EGZ acknowledges support from the University of Wisconsin-Madison and the hospitality of the University of Chicago,

where part of this review was written. SS acknowledges support from the National Science Foundation Early Career Award AST-1056780 and the University of Wisconsin-Madison Office of the Vice Chancellor for Research and Graduate Education Vilas Associate Award.

## LITERATURE CITED

## LITERATURE CITED

- Amato E. 2014. *International Journal of Modern Physics D* 23:1430013
- Andrews SM, Meyer DM, Lauroesch JT. 2001. *Ap. J. Lett.* 552:L73–L76
- Armstrong JW, Cordes JM, Rickett BJ. 1981. *Nature* 291:561–564
- Armstrong JW, Rickett BJ, Spangler SR. 1995. *Ap. J.* 443:209–221
- Audit E, Hennebelle P. 2005. *Astron. Astrophys.* 433:1–13
- Bannister K, Bignall H, Johnston S, Reynolds C, Stevens J, et al. 2016a. *The Astronomer’s Telegram* 8696
- Bannister KW, Stevens J, Tuntsov AV, Walker MA, Johnston S, et al. 2016b. *Science* 351:354–356
- Basu R, Rożko K, Lewandowski W, Kijak J, Dembska M. 2016. *MNRAS* 458:2509–2515
- Begum A, Stanimirović S, Goss WM, Heiles C, Pavkovich AS, Hennebelle P. 2010. *Ap. J.* 725:1779–1785
- Beresnyak A, Jones TW, Lazarian A. 2009. *Ap. J.* 707:1541–1549
- Bertoldi F, McKee CF. 1992. *Ap. J.* 395:140–157
- Bignall HE, Croft S, Hovatta T, Koay JY, Lazio J, et al. 2015. *Advancing Astrophysics with the Square Kilometre Array (AASKA14)* :58
- Biskamp D, Schwarz E, Zeiler A, Celani A, Drake JF. 1999. *Physics of Plasmas* 6:751–758
- Boissé P, Bergeron J, Prochaska JX, Péroux C, York DG. 2015. *Astron. Astrophys.* 581:A109
- Boldyrev S, Gwinn C. 2003. *Ap. J.* 584:791–796
- Boldyrev S, Königl A. 2006. *Ap. J.* 640:344–352
- Brogan CL, Zauderer BA, Lazio TJ, Goss WM, DePree CG, Faison MD. 2005. *Astron. J.* 130:698–710
- Burkhart B, Lazarian A, Balsara D, Meyer C, Cho J. 2015. *Ap. J.* 805:118
- Cha AN, Sembach KR. 2000. *Ap. J. Suppl.* 126:399–426
- Cho J, Lazarian A. 2003. *MNRAS* 345:325–339
- Cho J, Lazarian A. 2009. *Ap. J.* 701:236–252
- Cho J, Lazarian A, Vishniac ET. 2002. *Ap. J. Lett.* 566:L49
- Clark SE, Peek JEG, Putman ME. 2014. *Ap. J.* 789:82
- Clegg AW, Fey AL, Lazio TJW. 1998. *Ap. J.* 496:253–266
- Clifton TR, Frail DA, Kulkarni SR, Weisberg JM. 1988. *Ap. J.* 333:332–340
- Cognard I, Bourgois G, Lestrade JF, Biraud F, Aubry D, et al. 1993. *Nature* 366:320–322
- Coles WA, Kerr M, Shannon RM, Hobbs GB, Manchester RN, et al. 2015. *Ap. J.* 808:113
- Cordes JM, Weisberg JM, Boriakoff V. 1985. *Ap. J.* 288:221–247
- Cowie LL. 1975. *MNRAS* 173:429–436
- Cowie LL, McKee CF. 1977. *Ap. J.* 211:135–146
- Cox DP. 2005. *Annu. Rev. Astron. Astrophys.* 43:337–385
- Crawford IA. 2003. *Ap. Space Sci.* 285:661–675
- Danks AC, Sembach KR. 1995. *Astron. J.* 109:2627
- Danks AC, Walborn NR, Vieira G, Landsman WB, Gales J, García B. 2001. *Ap. J. Lett.* 547:L155–L159
- Davis RJ, Diamond PJ, Goss WM. 1996. *MNRAS* 283:1105
- Deshpande AA. 2000. *MNRAS* 317:199–204
- Deshpande AA, Dwarakanath KS, Goss WM. 2000. *Ap. J.* 543:227–234
- Deshpande AA, McCulloch PM, Radhakrishnan V, Anantharamaiah KR. 1992. *MNRAS* 258:19P–21P
- Dhawan V, Mirabel IF, Rodríguez LF. 2000. *Ap. J.* 543:373–385
- Diamond PJ, Goss WM, Romney JD, Booth RS, Kalberla PMW, Mebold U. 1989. *Ap. J.* 347:302–306
- Dickey JM, Crovisier J, Kazes I. 1981. *Astron. Astrophys.* 98:271–285
- Dickey JM, Lockman FJ. 1990. *Annu. Rev. Astron. Astrophys.* 28:215–261
- Dickey JM, McClure-Griffiths N, Gibson SJ, Gómez JF, Imai H, et al. 2013. *Publ. Astron. Soc. Aust.* 30:e003
- Dickey JM, Mebold U, Stanimirovic S, Staveley-Smith L. 2000. *Ap. J.* 536:756–772
- Dickey JM, Salpeter EE, Terzian Y. 1979. *Ap. J.* 228:465–474
- Dieter NH, Welch WJ, Romney JD. 1976. *Ap. J. Lett.* 206:L113–L115
- Dieter-Conklin N. 2009. *Astron. J.* 137:3920–3921
- Dirks C, Meyer DM. 2016. *Ap. J.* 819:45
- Draine BT. 1998. *Ap. J. Lett.* 509:L41–L44
- Draine BT, Roberge WG, Dalgarno A. 1983. *Ap. J.* 264:485–507

- Drury LO, Downes TP. 2012. *MNRAS* 427:2308–2313
- Dutta P, Chengalur JN, Roy N, Goss WM, Arjunwadkar M, et al. 2014. *MNRAS* 442:647–655
- Elmegreen BG, Scalo J. 2004. *Annu. Rev. Astron. Astrophys.* 42:211–273
- Faison MD, Goss WM. 2001. *Astron. J.* 121:2706–2722
- Faison MD, Goss WM, Diamond PJ, Taylor GB. 1998. *Astron. J.* 116:2916–2928
- Falkovich G, Lebedev V. 1997. *Single-point velocity distribution in turbulence*. In *eprint arXiv:chao-dyn/9708002*
- Ferrière K. 1998. *Ap. J.* 497:759–776
- Fiedler R, Dennison B, Johnston KJ, Waltman EB, Simon RS. 1994. *Ap. J.* 430:581–594
- Fiedler RL, Dennison B, Johnston KJ, Hewish A. 1987a. *Nature* 326:675–678
- Fiedler RL, Waltman EB, Spencer JH, Johnston KJ, Angerhofer PE, et al. 1987b. *Ap. J. Suppl.* 65:319–384
- Fiege JD, Pudritz RE. 2000. *MNRAS* 311:85–104
- Field GB, Goldsmith DW, Habing HJ. 1969. *Ap. J. Lett.* 155:L149
- Frail DA, Cordes JM, Hankins TH, Weisberg JM. 1991. *Ap. J.* 382:168–181
- Frail DA, Weisberg JM, Cordes JM, Mathers C. 1994. *Ap. J.* 436:144–151
- Genova R, Beckman JE, Bowyer S, Spicer T. 1997. *Ap. J.* 484:761
- Gerin M, Ruaud M, Goicoechea JR, Gusdorf A, Godard B, et al. 2015. *Astron. Astrophys.* 573:A30
- Goldreich P, Sridhar S. 1995. *Ap. J.* 438:763–775
- Goldsmith PF. 2013. *Ap. J.* 774:134
- Goss WM, Richards AMS, Muxlow TWB, Thomasson P. 2008. *ArXiv e-prints* 804
- Gwinn CR. 2001. *Ap. J.* 561:815–822
- Hacker TL, Brunner RJ, Lundgren BF, York DG. 2013. *MNRAS* 434:163–185
- Hamidouche M, Lestrade JF. 2007. *Astron. Astrophys.* 468:193–203
- Haverkorn M, Goss WM, eds. 2007. *SINS - Small Ionized and Neutral Structures in the Diffuse Interstellar Medium*, vol. 365 of *Astronomical Society of the Pacific Conference Series*
- Haverkorn M, Spangler SR. 2013. *Space Sci. Rev.* 178:483–511
- Heeschen DS. 1984. *Astron. J.* 89:1111–1123
- Heiles C. 1997. *Ap. J.* 481:193–204
- Heiles C, Stinebring D. 2007. *Observational Review of this SINS Meeting*. In *SINS - Small Ionized and Neutral Structures in the Diffuse Interstellar Medium*, eds. M Haverkorn, WM Goss, vol. 365 of *Astronomical Society of the Pacific Conference Series*
- Heiles C, Troland TH. 2003. *Ap. J.* 586:1067–1093
- Heiles C, Troland TH. 2004. *Ap. J. Suppl.* 151:271–297
- Heiles C, Troland TH. 2005. *Ap. J.* 624:773–793
- Hennebelle P, Audit E. 2007. *Astron. Astrophys.* 465:431–443
- Hennebelle P, Audit E, Miville-Deschênes MA. 2007. *Astron. Astrophys.* 465:445–456
- Hennebelle P, Falgarone E. 2012. *Astron. Astrophys. Rev.* 20:55
- Herbig GH. 1993. *Ap. J.* 407:142–156
- Herrera-Camus R, Bolatto A, Wolfire M, Ostriker E, Draine B, et al. 2017. *Ap. J.* 835:201
- HI4PI Collaboration, Ben Bekhti N, Flöer L, Keller R, Kerp J, et al. 2016. *Astron. Astrophys.* 594:A116
- Higdon JC. 1984. *Ap. J.* 285:109–123
- Higdon JC. 1986. *Ap. J.* 309:342–361
- Hill AS, Stinebring DR, Asplund CT, Berwick DE, Everett WB, Hinkel NR. 2005. *Ap. J. Lett.* 619:L171
- Hobbs LM, Ferlet R, Welty DE, Wallerstein G. 1991. *Ap. J.* 378:586–598
- Howes GG, Tenbarge JM, Dorland W. 2011. *Physics of Plasmas* 18:102305–102305
- Inoue T, Inutsuka Si. 2008. *Ap. J.* 687:303–310
- Inoue T, Inutsuka Si, Koyama H. 2006. *Ap. J.* 652:1331–1338
- Jauncey D, Bignall H, Kedziora-Chudczer L, Koay J, Lovell J, et al. 2016. *Galaxies* 4:62
- Jenkins EB, Tripp TM. 2011. *Ap. J.* 734:65
- Johnston S, Koribalski B, Wilson W, Walker M. 2003. *MNRAS* 341:941–947
- Kalberla PMW, Kerp J. 2016. *Astron. Astrophys.* 595:A37
- Kalberla PMW, Schwarz UJ, Goss WM. 1985. *Astron. Astrophys.* 144:27–36
- Kameswara Rao N, Lambert DL, Reddy ABS, Gupta R, Muneer S, Singh HP. 2017. *MNRAS* 467:1186–1192
- Kanekar N, Chengalur JN. 2001. *MNRAS* 325:631–635
- Kaplan DL, Tingay SJ, Manoharan PK, Macquart JP, Hancock P, et al. 2015. *Ap. J. Lett.* 809:L12
- Kim CG, Kim WT, Ostriker EC. 2008. *Ap. J.* 681:1148–1162
- Klessen RS, Heitsch F, Mac Low MM. 2000. *Ap. J.* 535:887–906
- Koyama H, Inutsuka S. 2002. *Ap. J. Lett.* 564:L97–L100
- Kritsuk AG, Norman ML, Padoan P, Wagner R. 2007. *Ap. J.* 665:416–431
- Lam MT, Cordes JM, Chatterjee S, Jones ML, McLaughlin MA, Armstrong JW. 2016. *Ap. J.* 821:66

- Lauroesch JT. 2007. *Optical Absorption Line Observations of Small Scale Interstellar Structure*. In *SINS - Small Ionized and Neutral Structures in the Diffuse Interstellar Medium*, eds. M Haverkorn, WM Goss, vol. 365 of *Astronomical Society of the Pacific Conference Series*
- Lauroesch JT, Meyer DM. 1999. *Ap. J. Lett.* 519:L181–L184
- Lauroesch JT, Meyer DM. 2002. *Probing the Diffuse Interstellar Medium at AU Scales*. In *American Astronomical Society Meeting Abstracts*, vol. 34 of *Bulletin of the American Astronomical Society*
- Lauroesch JT, Meyer DM. 2003. *Ap. J. Lett.* 591:L123
- Lauroesch JT, Meyer DM, Watson JK, Blades JC. 1998. *Ap. J. Lett.* 507:L89–L92
- Lazarian A, Beresnyak A, Yan H, Opher M, Liu Y. 2009. *Properties and Selected Implications of Magnetic Turbulence for Interstellar Medium, Local Bubble and Solar Wind*. 387
- Lazarian A, Pogosyan D. 2004. *Ap. J.* 616:943–965
- Lazio TJW, Brogan CL, Goss WM, Stanimirović S. 2009. *Astron. J.* 137:4526–4537
- Lazio TJW, Fey AL, Dennison B, Mantovani F, Simonetti JH, et al. 2000. *Ap. J.* 534:706–717
- Lazio TJW, Gaume RA, Claussen MJ, Fey AL, Fiedler RL, Johnston KJ. 2001a. *Ap. J.* 546:267–272
- Lazio TJW, Ojha R, Fey AL, Kedziora-Chudczer L, Cordes JM, et al. 2008. *Ap. J.* 672:115–121
- Lazio TJW, Waltman EB, Ghigo FD, Fiedler RL, Foster RS, Johnston KJ. 2001b. *Ap. J. Suppl.* 136:265–392
- Lee LC, Jokipii JR. 1975. *Ap. J.* 196:695–707
- Lee MY, Stanimirović S, Douglas KA, Knee LBG, Di Francesco J, et al. 2012. *Ap. J.* 748:75
- Lestrade JF, Rickett BJ, Cognard I. 1998. *Astron. Astrophys.* 334:1068–1084
- Li PS, McKee CF, Klein RI. 2006. *Ap. J.* 653:1280–1291
- Liszt H, Lucas R. 1996. *Astron. Astrophys.* 314:917–926
- Lithwick Y, Goldreich P. 2001. *Ap. J.* 562:279–296
- Mac Low MM, Balsara DS, Kim J, de Avillez MA. 2005. *Ap. J.* 626:864–876
- Marscher AP, Moore EM, Bania TM. 1993. *Ap. J. Lett.* 419:L101
- McClure-Griffiths NM, Stanimirovic S, Murray C, Li D, Dickey JM, et al. 2015. *Advancing Astrophysics with the Square Kilometre Array (AASKA14)* :130
- McEvoy CM, Smoker JV, Dufton PL, Smith KT, Kennedy MB, et al. 2015. *MNRAS* 451:1396–1412
- McKee CF. 2001. *Young supernova remnants: Issues and prospects*. In *AIP Conf. Proc. 565: Young Supernova Remnants*
- McKee CF, Cowie LL. 1977. *Ap. J.* 215:213–225
- McKee CF, Ostriker JP. 1977. *Ap. J.* 218:148–169
- McKee CF, Zweibel EG. 1992. *Ap. J.* 399:551–562
- Meyer DM. 1990. *Ap. J. Lett.* 364:L5–L8
- Meyer DM. 1994. *High Resolution HST and CCD Observations of Interstellar Absorption Lines*. In *The First Symposium on the Infrared Cirrus and Diffuse Interstellar Clouds*, eds. RM Cutri, WB Latter, vol. 58 of *Astronomical Society of the Pacific Conference Series*
- Meyer DM, Blades JC. 1996. *Ap. J. Lett.* 464:L179
- Meyer DM, Dirks C, Lauroesch JT. 2015. *A Survey of AU-Scale Na I Structure in the Diffuse ISM*. In *American Astronomical Society Meeting Abstracts*, vol. 225 of *American Astronomical Society Meeting Abstracts*
- Meyer DM, Lauroesch JT. 1999. *Ap. J. Lett.* 520:L103–L106
- Meyer DM, Lauroesch JT, Peek JEG, Heiles C. 2012. *Ap. J.* 752:119
- Minter AH, Balseer DS, Kartaltepe JS. 2005. *Ap. J.* 631:376–380
- Miville-Deschênes MA, Martin PG, Abergel A, Bernard JP, Boulanger F, et al. 2010. *Astron. Astrophys.* 518:L104
- Moore EM, Marscher AP. 1995. *Ap. J.* 452:671
- Münch G. 1953. *Publ. Astron. Soc. Pac.* 65:179
- Münch G. 1957. *Ap. J.* 125:42
- Murray CE, Stanimirović S, Goss WM, Dickey JM, Heiles C, et al. 2015. *Ap. J.* 804:89
- Murray CE, Stanimirović S, Kim CG, Ostriker EC, Lindner RR, et al. 2017. *Ap. J.* 837:55
- Ossenkopf V, Mac Low MM. 2002. *Astron. Astrophys.* 390:307–326
- Pan K, Federman SR, Welty DE. 2001. *Ap. J. Lett.* 558:L105–L108
- Pen UL, King L. 2012. *MNRAS* 421:L132–L136
- Phillips JA, Wolszczan A. 1991. *Ap. J. Lett.* 382:L27–L30
- Points SD, Lauroesch JT, Meyer DM. 2004. *Publ. Astron. Soc. Pac.* 116:801–818
- Pushkarev AB, Kovalev YY, Lister ML, Hovatta T, Savolainen T, et al. 2013. *Astron. Astrophys.* 555:A80
- Rao NK, Muneer S, Lambert DL, Varghese BA. 2016. *MNRAS* 455:2529–2550
- Ray A, Loeb A. 2017. *Ap. J.* 836:135
- Rickett B, Johnston S, Tomlinson T, Reynolds J. 2009. *MNRAS* 395:1391–1402
- Rickett BJ. 1970. *MNRAS* 150:67
- Rickett BJ. 1977. *Annu. Rev. Astron. Astrophys.* 15:479–504
- Rickett BJ. 1990. *Annu. Rev. Astron. Astrophys.* 28:561–605



- Rickett BJ, Coles WA, Bourgois G. 1984. *Astron. Astrophys.* 134:390–395
- Rickett BJ, Quirrenbach A, Wegner R, Krichbaum TP, Witzel A. 1995. *Astron. Astrophys.* 293:479–492
- Romani RW, Blandford RD, Cordes JM. 1987. *Nature* 328:324–326
- Roy N, Chengalur JN, Dutta P, Bharadwaj S. 2010. *MNRAS* :L33+
- Roy N, Minter AH, Goss WM, Brogan CL, Lazio TJW. 2012. *Ap. J.* 749:144
- Scalo J, Elmegreen BG. 2004. *Annu. Rev. Astron. Astrophys.* 42:275–316
- Scheuer PAG. 1968. *Ap. J. Lett.* 151:L139
- Scheuer PAG, Tsytovich VN. 1970. *Ap. Lett.* 7:125
- Shishov VI, Smirnova TV, Sieber W, Malofeev VM, Potapov VA, et al. 2003. *Astron. Astrophys.* 404:557–567
- Shraiman BI, Siggia ED. 2000. *Nature* 405:639–646
- Simon JD, Shappee BJ, Pojmanski G, Montet BT, Kochanek CS, et al. 2017. *ArXiv e-prints*
- Smith KT, Fossey SJ, Cordiner MA, Sarre PJ, Smith AM, et al. 2013. *MNRAS* 429:939–953
- Smith KW, Terry PW. 2011. *Ap. J.* 730:133
- Smoker JV, Bagnulo S, Cabanac R, Keenan FP, Fossati L, et al. 2011. *MNRAS* 414:59–75
- Spitzer LJ. 1978. *Physical processes in the interstellar medium*. New York, USA: J. Wiley & Sons, Inc
- Stanimirović S, Weisberg J, Dickey JM, de la Fuente A, Devine K, et al. 2003. *Ap. J.* 592:953
- Stanimirović S. 2009. *Space Sci. Rev.* 143:291–301
- Stanimirović S, Murray CE, Lee MY, Heiles C, Miller J. 2014. *Ap. J.* 793:132
- Stanimirović S, Weisberg JM, Hedden A, Devine KE, Green JT. 2003. *Ap. J. Lett.* 598:L23
- Stanimirović S, Weisberg JM, Pei Z, Tuttle K, Green JT. 2010. *Ap. J.* 720:415–434
- Stinebring D. 2007. *Pulsar Scintillation Arcs and the Ionized ISM*. In *SINS - Small Ionized and Neutral Structures in the Diffuse Interstellar Medium*, eds. M Haverkorn, WM Goss, vol. 365 of *Astronomical Society of the Pacific Conference Series*
- Stutzki J, Bensch F, Heithausen A, Ossenkopf V, Zielinsky M. 1998. *Astron. Astrophys.* 336:697–720
- Tennekes H, Lumley JL. 1972. *First Course in Turbulence*
- Terry PW, Smith KW. 2007. *Ap. J.* 665:402–415
- Terry PW, Smith KW. 2008. *Physics of Plasmas* 15:056502–056502
- Tilley DA, Balsara DS. 2011. *MNRAS* 415:3681–3692
- Tuntsov AV, Bignall HE, Walker MA. 2013. *MNRAS* 429:2562–2568
- Tuntsov AV, Stevens J, Bannister KW, Bignall H, Johnston S, et al. 2017. *MNRAS* 469:5023–5032
- van Haasteren R. 2014. *Gravitational Wave Detection and Data Analysis for Pulsar Timing Arrays*
- van Loon JT, Bailey M, Tatton BL, Maíz Apellániz J, Crowther PA, et al. 2013. *Astron. Astrophys.* 550:A108
- Walker M, Wardle M. 1998. *Ap. J. Lett.* 498:L125–L128
- Wardle M, Walker M. 1999. *Ap. J. Lett.* 527:L109–L112
- Warhaft Z. 2000. *Annual Review of Fluid Mechanics* 32:203–240
- Watson JK, Meyer DM. 1996. *Ap. J. Lett.* 473:L127
- Weisberg JM, Johnston S, Koribalski B, Stanimirović S. 2005. *Science* 309:106–110
- Weisberg JM, Rankin J, Boriakoff V. 1980. *Astron. Astrophys.* 88:84–93
- Weisberg JM, Stanimirović S. 2007. *Pulsar Studies of Tiny-Scale Structure in the Neutral ISM*. In *SINS - Small Ionized and Neutral Structures in the Diffuse Interstellar Medium*, ed. M. Haverkorn & W. M. Goss, vol. 365 of *Astronomical Society of the Pacific Conference Series*
- Weisberg JM, Stanimirović S, Xilouris K, Hedden A, de la Fuente A, et al. 2008. *Ap. J.* 674:286–294
- Welty DE. 2007. *Ap. J.* 668:1012–1027
- Welty DE, Simon T, Hobbs LM. 2008. *MNRAS* 388:323–334
- Witzel A, Heeschen DS, Schalinski C, Krichbaum T. 1986. *Mitteilungen der Astronomischen Gesellschaft Hamburg* 65:239
- Wolfire MG. 2015. *Highlights of Astronomy* 16:600–602
- Wolfire MG, McKee CF, Hollenbach D, Tielens AGGM. 2003. *Ap. J.* 587:278–311
- Wright JT, Sigurdsson S. 2016. *Ap. J. Lett.* 829:L3
- Zhdankin V, Boldyrev S, Mason J. 2017. *MNRAS* 468:4025–4029
- Zhdankin V, Uzdensky DA, Boldyrev S. 2015. *Physical Review Letters* 114:065002
- Zhdankin V, Uzdensky DA, Perez JC, Boldyrev S. 2013. *Ap. J.* 771:124
- Zweibel E. 2005. *On plasma turbulence and dissipation scales in the ISM*. In *SINS - Small Ionized and Neutral Structures in the Diffuse Interstellar Medium*
- Zweibel EG. 2002. *Ap. J.* 567:962–970
- Zweibel EG. 2015. *Ambipolar Diffusion*. In *Magnetic Fields in Diffuse Media*, eds. A Lazarian, EM de Gouveia Dal Pino, C Melioli, vol. 407 of *Astrophysics and Space Science Library*
- Zweibel EG, Brandenburg A. 1997. *Ap. J.* 478:563–568
- Zweibel EG, Heiles C. 1997. *Nature* 385:131–136